An Investigation on Passive Intermodulation Generated by Antenna Contact

by

Forhad Hasnat

A thesis
presented to the University of Waterloo
in fulfillment of the
thesis requirement for the degree of
Masters of Applied Science
in
Electrical and Computer Engineering

Waterloo, Ontario, Canada, 2017

Author's Declaration

I hereby declare that I am the sole author of this thesis. This is a true copy of the thesis, including any required final revisions, as accepted by my examiners.

I understand that my thesis may be made electronically available to the public.

Abstract

In modern day handheld cellular devices, low-profile is a key design target. In addition, with the introduction of 4G protocols, the number of cellular bands has increased significantly and the simultaneous transmission of multiple bands is more common than ever before. These requirements lead to challenges for designers as the close proximity of passive devices (e.g., antenna) to active devices (e.g., radio) can lead to additional distortions in the signal. Due to the overlapping nature of many frequency bands, harmonics/intermodulation distortion can seriously degrade the receiver sensitivity of coexisting radios. One way in which this can occur is that the antenna metal-to-metal contact can generate a metal-insulator/semiconductor junction due to surface roughness. If the gap between the layers is small enough, it can generate a tunnel current through the gap. This tunnel current has a non-linear I-V characteristic. For this reason, it is important to investigate the non-linearity caused by passive sources in antenna structures.

Non-linearity caused by passive sources can produce significant distortion for active devices with high transmit power or low receive sensitivity requirements. The aim of this research was to devise a measurement technique to study the unknown nonlinear behavior of radio frequency antenna metal-to-metal contacts. Issues related to the measurement of low-level distortion were investigated. As part of this research, a measurement setup was developed to measure low-level distortion. Measurements made showed that intermodulation caused by metal-to-metal contact in the antenna structure can degrade receiver sensitivity significantly. This thesis also discusses an approach to modelling nonlinear relationships, based on the measurements made with the new test setup.

Acknowledgements

I have the utmost respect and deepest gratitude to my supervisor, Dr. Safieddin Safavi-Naeini. Without his relentless support and direction, I would not have been able to pursue this research.

I would also like to convey my thanks to my co-supervisor Dr. Nagula Sangary. From his busy schedule, he has allocated time to provide invaluable suggestions and directions.

I would like to thank Dr. Slim Boumaiza for kindly accepting to attend my seminar and review my thesis. I was lucky to attend his lecture on “Nonlinear RF Devices” which lent me the major foundation for my research.

I would also like to thank Dr. George Shaker who kindly accepted to review my thesis and to provide valuable feedback.

Working full time while doing this research as a part-time student, I had to steal lots of time from my family. I am grateful to my father for always trusting me, my mother for dedicating her life to me, my sister and brothers for being such wonderful beings and my supportive family for their patience. I owe great thanks to my wife for keeping patience, raising our two daughters with very little support from me. Without her help, I would not have been able to pull off my graduate studies.

Finally, I would like to thank the Almighty God for giving me a wonderful family, and for allowing me to pursue my dream.

Table of Contents

List of Figures

List of Tables

Chapter 1
Introduction

1.1 Motivation

Making communication possible across the globe is considered one of the major scientific and engineering achievements of the last century. The ability to communicate over-the-air (OTA) has given mankind the ability to transfer information around the world, process it and use it at phenomenal rates. Today's commercial modems have the capacity to download and process data at an incredible speed of 1 Gbps—truly a sensational achievement [1]. In addition to the brilliant technological breakthroughs and lifesaving applications that communications technologies have enabled, the communication systems industry itself is a trillion-dollar market sector [2]. This economic engine continues to drive research and promote constant innovation to make communications technologies better.

Cell phones today are among the most complex electronic devices on the planet. Consumers demand packaging—a thin, slick body with a shiny metallic look—that is not just a fashion trend but a substantial design challenge for radio frequency (RF) engineers. High-end cell phones with embedded cameras with resolutions of over 40-megapixels can take and process 4K videos and transmit and receive these highly dense data packets in the blink of an eye [3]. Whether you are in a jet or in a car, there is an expectation of a seamless communication link and high-speed data transfer capability. The challenge to package almost limitless hardware and software functionally into stylish palm size devices, requires increasingly sophisticated levels of design. Accomplishing these divergent goals simultaneously is the biggest challenge facing communication engineers today in system level platforms like cell phones.

In this thesis, an investigation of system-level RF challenges from a multi radio coexistence perspective is undertaken. The mechanism by which receiver sensitivity is degraded in the presence of a jammer is studied. Passive nonlinearity is identified as a dominating source of receiver degradation. A test fixture and intermodulation distortion (IMD) measurement setup are developed. Measured data analysis shows that passive sources can generate enough IMD to cause receiver sensitivity degradation.

1.2 Multi-radio System Challenges

In the following chapters, handheld device system-level RF design challenges are discussed in detail. The specific issue/scenario on which this thesis is focused is the simultaneous transmission and reception of data using multiple radios within a handheld mobile device. Figure 1.1 below shows in a typical network how multiple devices can be connected [4]. At the same time, same unit can be connected to multiple radio stations.

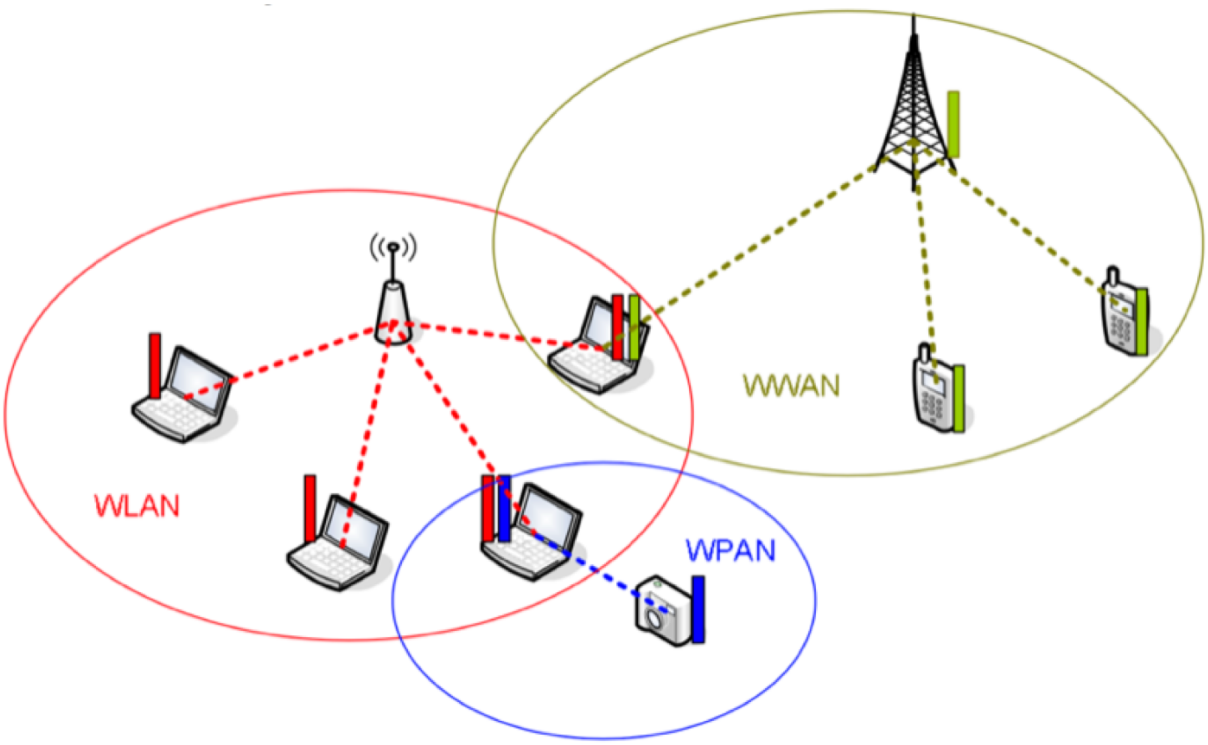

Figure 1.1 Multiple Radio Coexistence Scenarios

The sensitivity of the receiver plays a critical role in maintaining the radio link within any wireless communication system. While receiver sensitivity itself is a very popular topic of research, the focus has been on analyzing receiver sensitivity under jammer signal operation. In state-of-the-art handheld devices, different radios have different signal transmission levels and different sensitivity criteria, based on their application. As a result, signal levels in transmitters and receivers can simultaneously be anywhere between +33dBm and -130dBm [5], [6]. This means that there can be a dynamic range of almost 160 dB, something that is extremely challenging to mitigate.

Many of these problems can be solved with state-of-the-art filtering, electromagnetic shielding, software mitigation etc. Within an individual radio sub-system, the software mitigation approach is well understood. However, the system level implementation of multiple radio platforms brings its own challenges, many of which remain unresolved. Until recently, many of these challenges were ignored and not subjected to analysis.

The introduction and implementation of fourth generation (4G) technologies has crowded the frequency spectrum to such an extent that almost all bands will find a second band with which to interfere if they are operating simultaneously. The nonlinearity of active components (e.g., power amplifiers, mixers, switches etc.) has been correctly identified as the primary contributor to these so-called intentional noise sources. Plenty of good work has been done to improve the linearity of active components. However, at the system level, it has been found that active components are not the only dominant source of noise. The generation of passive intermodulation (PIM) has been identified as a critical contributor, found to be more prominent in radiated noise emission measurements than in conducted measurements [7]. Intermodulation generated by passive components is not a new concept; it has been well researched in relation to satellite and base-station communications [8]. However, PIM mechanisms have not been well explored in relation to low-profile handheld devices where there are significantly different design criteria and foci. This thesis describes research undertaken to investigate PIM mechanisms and how they relate to low-profile, low-power handheld mobile devices. A novel approach to isolating and measuring PIM within such design constraints is proposed. Several critical contributors to PIM generation in an RF system platform are identified, one of which is explained in detail in the following chapters.

1.3 Thesis Organization

Chapter Two provides the context for the research and explains relevant concepts. It includes a detailed description of RF multi-radio coexistence criteria. Potential user impacts are discussed as well. A typical radio system diagram of a modern cell phone is presented and different critical areas are discussed. The basics of intermodulation distortion (IMD) and receiver sensitivity are outlined in Chapter Two, as well as the different mechanisms of sensitivity degradation in RF sub-systems. How performance varies with the external jammer signal is also explained.

Later parts of this chapter give an overview of the basic mechanism of PIM generation. Physical properties are explained from the application perspective in order to enable the concept of a

complicated radio system platform to be engineered. Interesting and related work from other researchers is discussed. Different types of RF antennas used in cell phones are described and the ways in which different designs can impact the overall system's linearity performance are briefly mentioned. Antenna contacts are identified as a critical source of PIM and challenges in rooting out the cause of PIM are discussed.

Chapter Three, discusses the design of a highly linear test sample kit and fixture for measuring PIM effect. The biggest challenge facing PIM measurement is to ensure the test setup is linear enough to identify the nonlinear response of the complete test kit. In this chapter, the three dimensional full wave simulation used to analyze the linear response of the test kit is explained.

In Chapter Four, a novel test setup is proposed to measure and analyze PIM in low power handheld devices. Measurement challenges and practical limitations related to crucial measurement equipment are pointed out. Experimental data are presented and discussed. The attempt to measure large signal S-parameters, and some fundamental challenges to this measurement, are also discussed.

Chapter Five provides conclusions based on the findings of the research, and outlines directions for future work in this area.

Chapter 2

Background and Literature Review

2.1 Coexistence Frequency Spectrum

Continued growth in new mobile applications, has resulted in the need for cell phones to perform multiple tasks simultaneously. Because of this, multiple radio coexistence is now a mandatory design requirement. Today's cell phones integrate a number of technologies including cellular, WLAN, GPS and Bluetooth. These technologies utilize RF bands that range anywhere between 500 MHz and 6 GHz. It is not uncommon to have over 20 different RF bands in a single cell phone. With the inclusion of 4G technologies, it is now guaranteed that a cell phone will have at least two radios on simultaneously, requiring design-for-coexistence strategies. Figure 2.1 below, summarizes the most common technologies found in cell phones today [4].

Usage	Radio	Band
WAN	Cellular (GSM, CDMA, GPRS)	824-894 MHz, 880-960 MHz, 1770-1880 MHz, 1850-1990 MHz
	UMTS (W-CDMA,CDMA 2000, 1xEV-DO)	1920-1980 MHz, 2110-2170 MHz
	802.16 (WiMAX)	2300-2400 MHz, 2496- 2690 MHz, 3300- 3800 MHz
LAN	802.11 (WiFi)	2402-2483 MHz
PAN	802.15.1 (Bluetooth)	2402-2483 MHz
Location Service	GPS	1575.42 MHz

Figure 2.1 Frequency Allocation of Different Wireless Technologies

2.2 Coexistence Use Cases

Coexistence scenarios are typically user-case driven or application dependent. Some cell phone users, for example, watch television and talk at the same time while others may be heavy headset users and use Bluetooth technology and standard voice cellular technology. Below, there is a summary of some of the more common design-for-coexistence scenarios.

- GPS-LTE Cellular Coexistence [9]: User is using cell phone GPS technology for navigation and LTE technology for video/audio streaming, simultaneously. This would be a potential GPS-cellular coexistence concern and a very typical scenario to occur while driving.
- Bluetooth-Cellular Coexistence [10]: User is using a wireless hands-free headset which relies on Bluetooth technology. User may be receiving a call over the cell phone, which is connected to a cellular network, while using a Bluetooth headset to talk over the phone. This would be a potential Bluetooth-cellular coexistence concern.
- WiFi-Cellular Coexistence [4]: User is using a cell phone as a WiFi hotspot, while connected to an LTE network for data coverage. This is a typical WiFi-cellular coexistence concern.
- Carrier Aggregation-3GPP Coexistence [11]: In order to increase the bandwidth and data rate, 3GPP (Third Generation Partnership Project) standards permit multiple LTE bands to operate simultaneously. This feature is called carrier aggregation. In this case, the IMD of two transmit bands and one of the receive bands frequently overlap, resulting in receiver sensitivity degradation. For example, the LTE band 5 (824 MHz–849 MHz) and band 13 (777 MHz–787 MHz) transmit bands can generate IMD that falls into the LTE band 5 (869 MHz–894 MHz) receive band. This results in receiver sensitivity degradation, a major design-for-coexistence concern.
- Data-Voice Coexistence [11]: It is not uncommon for a cellular phone platform to receive data and voice at the same time. This protocol is called “simultaneous voice and LTE” or SVLTE. Because these bands are operating at the same time, there is a potential for sensitivity degradation of the receive band. One notable instance is when the LTE band 13 transmitter (782 MHz, data) and the CDMA BC0 (827 MHz, voice) are both in use. In this case, the mixing can generate IMD within the CDMA receiver band (872 MHz).
- Gateway-WiFi-Radio Coexistence [4]: A residential gateway that has both in-bound (WiFi) and out-bound radios would also face coexistence challenges.

- WiFi Monitor-Cellular Network Coexistence [4]: A mobile device that uses WiFi to display to a remote monitor, can receive data (that it displays) using the cellular network.

Not having a standardized approach to coexistence is a major design problem for the industry and designers. The number of possible coexistence combinations that could result from the simultaneous use of different voice, video and data protocols and technologies are too numerous to deal with in an easily standardized way. This has resulted in customized and non-standardized design-for-coexistence approaches.

2.3 Coexistence Performance Degradation Mechanisms

A generalized approach to designing for coexistence scenarios addresses coexistence from the viewpoint of victim and aggressor, even though coexistence can be categorized in a variety of other ways [10]. A discussion of each of the types framed from the user case point of view—aggressor out of band (OOB) noise, aggressor harmonics/IMD, aggressor-aggressor harmonics—follows below.

2.3.1 Aggressor Out Of Band Noise Increases Victim Receiver Noise Floor

This scenario is more common during simultaneous cellular and WLAN operation. The WLAN ISM band operates between 2.4 GHz and 2.485 GHz. A number of cellular bands operate adjacent to the 2.4 GHz band. Figure 2.2 below shows the bands adjacent to the 2.4 GHz ISM band [12].

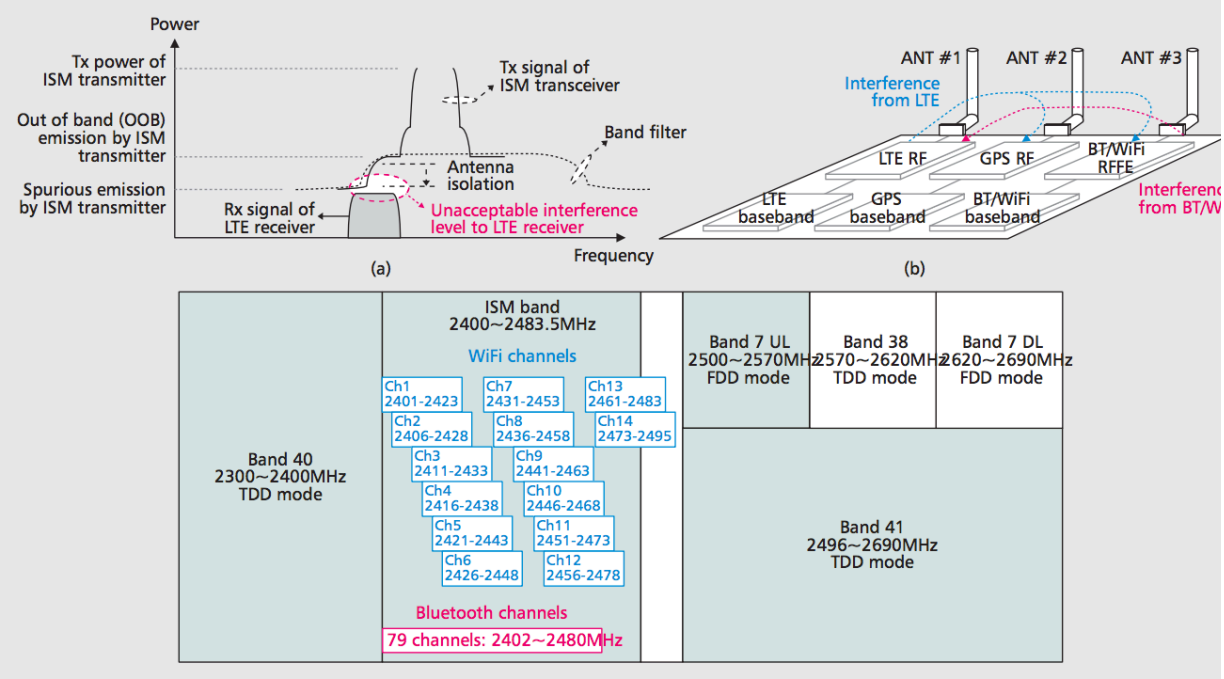

Figure 2.2 LTE-ISM Band Coexistence Concerns

Because WiFi and Bluetooth technologies share the same frequency band, OOB noise from the LTE high bands (B38, B41) results in a coexistence design issue for both WiFi and Bluetooth channels. Similarly, when either WiFi or Bluetooth is on, sensitivity degradation becomes an issue within the cellular channel [13].

2.3.2 Aggressor Harmonics/Intermodulation Distortion Increases Victim Receiver Noise Floor

Nonlinearity from active and passive components is a major source of unwanted harmonics. Many cellular bands with transmit frequencies between 800 MHz and 824 MHz have a third harmonic component which falls into the WiFi and Bluetooth bands. Often the cell phone and WiFi transmit bands mix to create a nonlinear component and an IMD product that is within the cellular receive band.

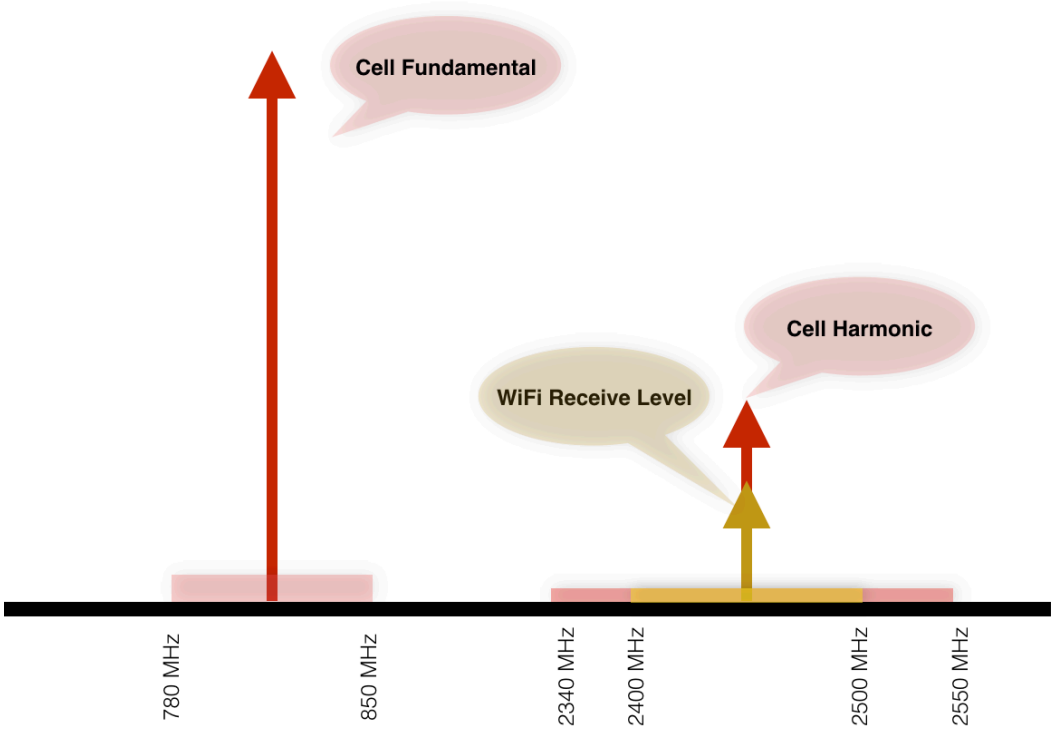

Figure 2.3 Cellular Harmonics Fall Within WiFi Band

Power amplifier nonlinearity generates high-level harmonics in the transmit chain. Fortunately, adequate filtering can reduce these high-level harmonics to an acceptable level. Unlike in the OOB case where the frequency separation is very narrow, it is possible to achieve the required rejection for harmonically related bands. However, in system level design, the component level link budget has limitations. Typically, RF components are matched to a 50-ohm impedance. While this matching is controllable at the component level, it is extremely difficult to control at the system level. The main reason is the presence of the antenna. Since antenna impedance is a wideband function of frequency it is not possible to guarantee matching with a 50-ohm impedance. As a result, harmonic levels can be different at the systems level compared to the conducted level. The source of this nonlinearity is the active components in the transmitter. However, there can also be a passive source of nonlinearity within the antenna sub-system. This passive source needs to be better understood. The sources of PIM are discussed in more detail in subsequent chapters.

2.3.3 Aggressor-Aggressor Harmonics Cause Victim Receiver Blocking

Receiver blocking compromises the linearity of the low noise amplifier (LNA), and this results in a sensitivity degradation in the receiver. One source of receiver blocking is an increased receiver noise floor, a direct result of reciprocal mixing. Low band second harmonics can impact a GPS receiver's blocking performance [37]. The cellular high-band and the 2.4 GHz WiFi band can impact each other's receiver performance, most often occurring when one channel is transmitting while the other is receiving. The GPS case and the OOB case differ in regards to the causes of receiver blocking. In the case of OOB interference, there is a wideband elevation of the noise floor resulting in LNA saturation (mixing products added to the mixer in the receiver chain) that causes blocking. In addition, active and passive nonlinear sources increase the jammer level, leading to receiver blocking. A simplified block diagram of a typical cell phone coexistence scenario is shown below in Figure 2.4.

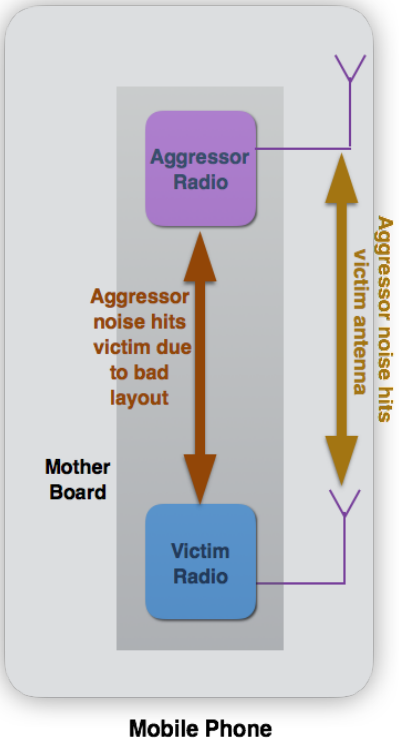

Figure 2.4 Noise Leakage Mechanism in Mobile Phone

Noise propagation design-for-coexistence issues can be divided into two primary categories: conducted and radiated noise. If noise travels through the main motherboard from an aggressor radio to a victim radio (due to poor layout), it is considered a conducted issue. However, if noise is radiated

by an aggressor antenna and the victim radio picks it up, it is considered to be a radiated issue [10]. Both issues require careful consideration when designing.

2.4 Critical Receiver System Parameters

The different receiver specifications and performance requirements are summarized in Figure 2.5 [11]. Each one is discussed in more detail below, in terms of coexistence-proof multi-radio design.

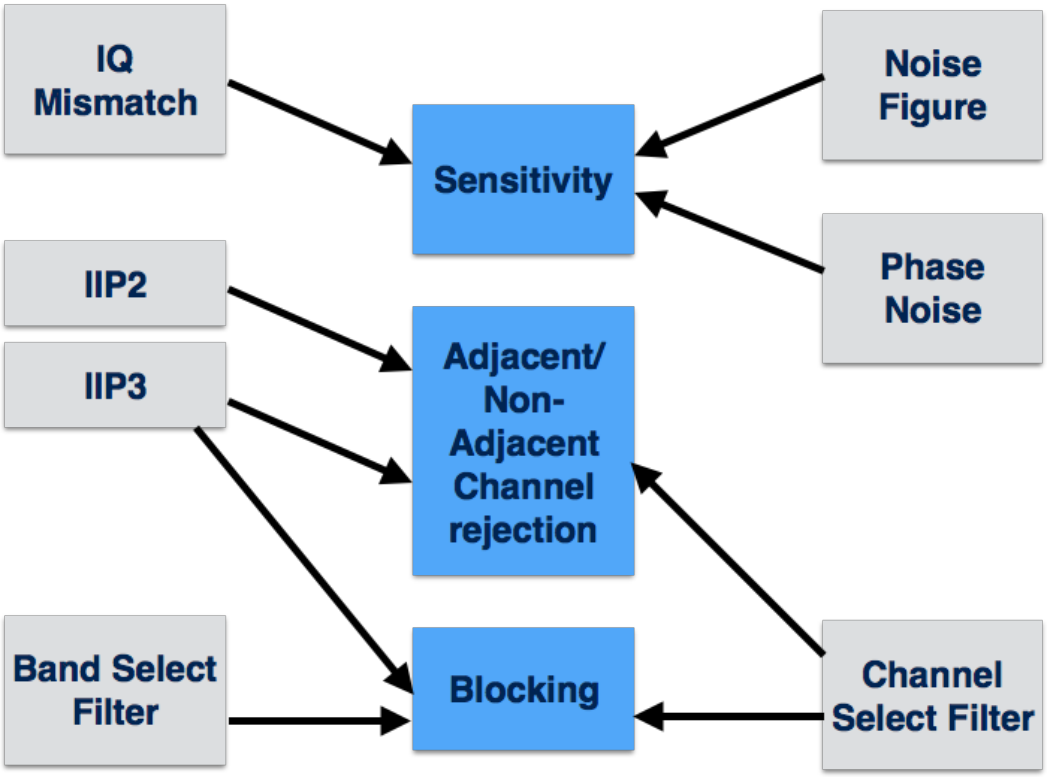

Figure 2.5 Receiver Sensitivity Degradation in the Presence of an External Jammer

2.4.1 Receiver Sensitivity

Receiver sensitivity is one of the most important performance specifications. It is defined as the minimum signal level that is required by the receiver to maintain the packet error rate below a certain level over the number of bytes specified by the system [13]. For example, the 802.11a standard defines sensitivity as the minimum signal required by an antenna connector to have a packet error rate of less than 10% at a PHY sub-layer service data unit (length of 100 bytes). Equation 2.1 [13], shows

the relation of sensitivity (P_{sen}) to the noise figure (NF), thermal noise (P_{noise}) and signal-to-noise ratio (SNR'):

$$P_{sen} = P_{noise} + NF + SNR' \quad (2.1)$$

$$where\ SNR' = \frac{P_s}{P_N + < |N_i|^2 >} = \frac{SNR}{1 + SNR \times F_{ici}}$$

$$where\ SNR = \frac{P_s}{P_N}\ and$$

$$F_{ici} = < |N_i|^2 > / P_s$$

2.4.2 Signal to Noise Ratio

In the signal-to-noise ratio calculation shown above, P_s is the average signal power and P_N is the average common phase noise power. The common phase noise power is a constant error for all subcarriers (relevant for OFDM systems). The information pilot signal can be used to correct phase induced error. However, there is a component of noise for which there is no compensating. Inter-carrier interference is quite challenging to correct for, given a large number of subcarriers [13]. In equation 2.1, inter-carrier interference is denoted by N_i, and F_{ici} is the phase noise density. This equation shows the importance of the phase of noise in the sensitivity calculation.

2.4.3 Thermal Noise

Thermal noise is generated due to the random motion of electrons and is proportional to temperature and signal bandwidth. The thermal noise power, P_{noise}, is given by the follow equation [14]:

$$P_{noise} = \kappa \times \mathrm{T} \times B$$

where κ is the Boltzmann constant, T is the temperature, and B is the bandwidth. At room temperature, $\mathrm{P_{noise}} = -174\ \mathrm{dBm/Hz}$.

2.4.4 Noise Figure

The noise figure is the ratio of signal-to-noise ratio degradation of a system as a signal travels from one end of the receiver chain to the other (equation 2.2).

$$NF = \frac{SNR_{in}}{SNR_{out}} \quad (2.2)$$

In a typical RF receiver, there are chains of active and passive RF components. Harold Friis defined the total system noise figure mathematically as follows [36]:

$$NF_{total} = NF_1 + \frac{NF_2 - 1}{G_1} + \frac{NF_3 - 1}{G_1 G_2} + \cdots + \frac{NF_n - 1}{G_1 G_2 \ldots G_{n-1}} \tag{2.3}$$

where NF_{total} is the equivalent input noise factor (linear), F_i is the stage noise factor (linear) and G_i is the stage gain (linear). The overall system's noise figure is dominated by the first component of the receiver chain on the antenna side. Typically, the front-end LNA drives the overall noise figure. Phase noise degradation adversely impacts sensitivity performance. LNA gain, on the other hand, improves sensitivity. This is because higher LNA gain lowers the systemic noise figure. Balancing these two factors is the key to coexistent-capable receiver design. For example, assuming an ambient noise level for an AWGN channel is -114 dBm/MHz, if NF is the noise figure of a victim radio and LS is the allowed sensitivity degradation of the victim radio induced by aggressor noise from a second radio or source, then noise at the victim input should be less than [10]

$$Aggressor\ noise = -114 + 10\ log_{10}\left(10^{\frac{LS}{10}} - 1\right) + NF \tag{2.4}$$

For example, if the allowed degradation is 3 dB, then the noise level has to be less than -106 dBm, assuming an 8 dB noise figure of the victim radio [10].

2.4.5 Adjacent/Nonadjacent Channel Rejection

Channel rejection filtering is critical to eliminating noise in an outside victim band. Noise can be adjacent or nonadjacent to the victim band. If the noise level is too high, even if it is OOB of the victim band, it can saturate the victim receiver. It is important to know the linearity specifications of the radio. The primary figures to measure linearity are the 1 dB compression point P_{1dB}, and the IMD [15].

2.4.6 1-dB Compression Point

Amplifiers when operated under small signals conditions in the linear region are expected to have a specific linear gain at a specific operating temperature and frequency. If the input signal level is varied, the gain should not vary. However, as the input changes from a small signal to a large signal region the gain does not change linearly. As a result, the gain is no longer linear and it starts to decrease. At a certain input level, the gain reduces by 1 dB. That level is called the 1-dB compression

point [15]. Since gain is reduced, the noise figure of the system increases and the sensitivity degrades. If the OOB noise is high enough to drive the LNA to operate in the nonlinear region, it causes receiver sensitivity degradation.

2.4.7 Intermodulation Distortion

The IMD product is the mixing product of multiple signals when they enter a nonlinear component simultaneously. Second (2^{nd}) order nonlinearity can be correlated with the 2^{nd} order input intercept point (IIP2) and the 3^{rd} order with IIP3. The IMD product and the interpretations of IIP2, IIP3 are indications of the linearity of a system or component.

The measurement of IIP2, IIP3 is quite similar. Two-tone (2-tone; same magnitude) signals are applied to a nonlinear device. The 2^{nd} and 3^{rd} order products are measured for IIP2 and IIP3, respectively. The input power is swept across a few points, enough to plot a line. The fundamental output is measured with the same input sweep. Individual sets of points are then connected to form lines. For each of the fundamental, 2^{nd} order and 3^{rd} order outputs, one line is determined. The 2^{nd} order line crosses the fundamental line at a particular point. The input power level at that point is called IIP2. Similarly, the 3^{rd} order and fundamental lines intersect at a point. The input power level at that point is called IIP3. Figure 2.6 below, shows the interpretation of the IIP2, IIP3, and 1-dB compression points.

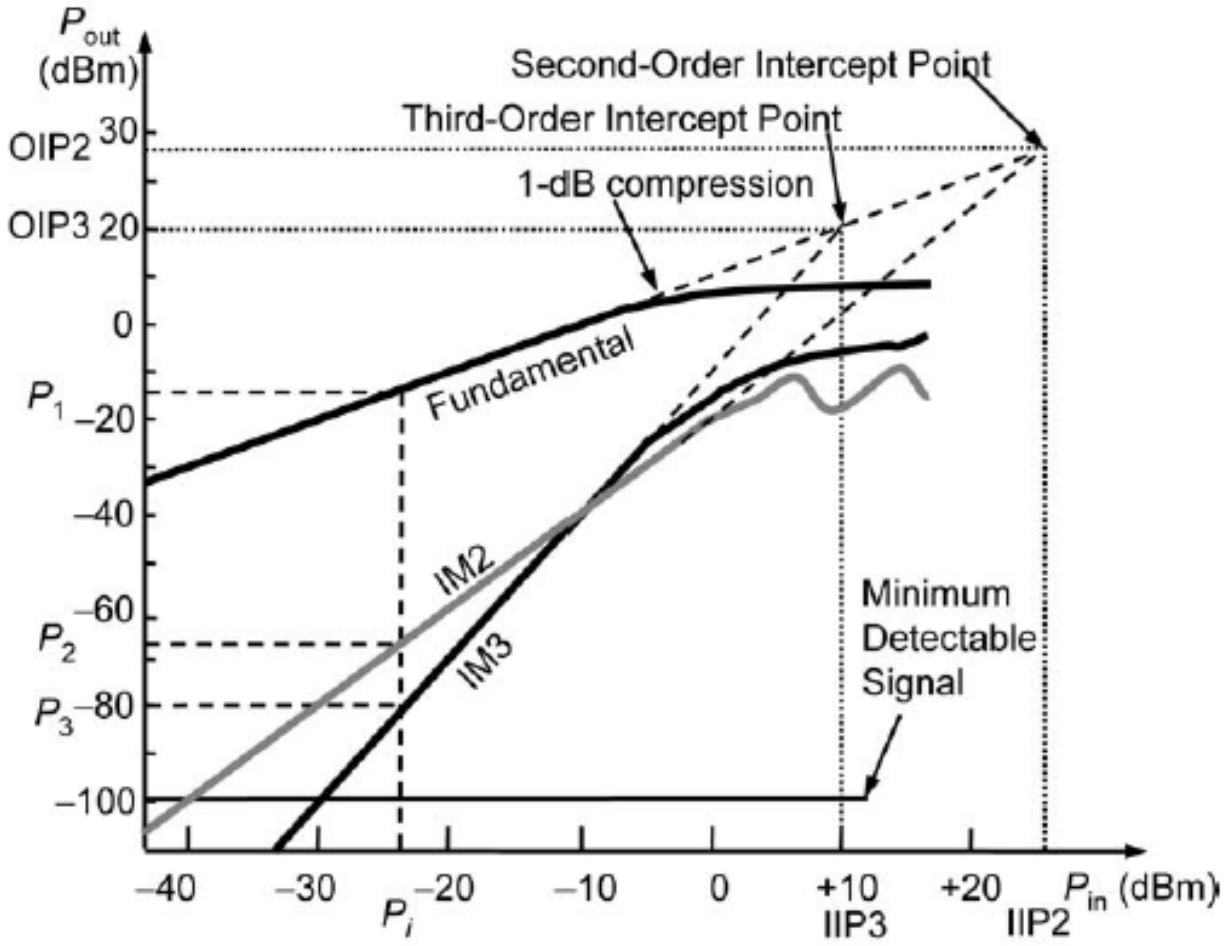

Figure 2.6 Important Nonlinear Parameters

IMD products are found mathematically with the power series expansion of trigonometric functions. Any nonlinear element can be described by a Taylor-series expansion [15] such as:

$$P(s) = a_0 + a_1.s + a_2.s^2 + a_3.s^3 + \cdots$$

Here, *s* is the input signal and *P(s)* is its transfer function. Examining the powers of *s* first, and assuming that the input signal consists of 2-tones as below:

$$S(t) = B_1.\cos(\omega_1 t) + B_2.\cos(\omega_2 t)$$

The trigonometric expansion of the 3rd power terms yield:

$$s^3(t) = B_1^3.cos^3(\omega_1 t) + B_2^3.cos^3(\omega_2 t) + 3.B_1^2.B_2.cos^2(\omega_1 t).\cos(\omega_2 t) + 3.B_2^2.B_1.cos^2(\omega_2 t).\cos(\omega_1 t) \quad (2.5)$$

With trigonometric expansion, it can be shown that the first two terms describe the 3rd order harmonics term for each of the input signals. The second and third terms describe intermodulation terms. Intermodulation signals are shown in Figure 2.7 below, where f_1 and f_2 are input signals [16].

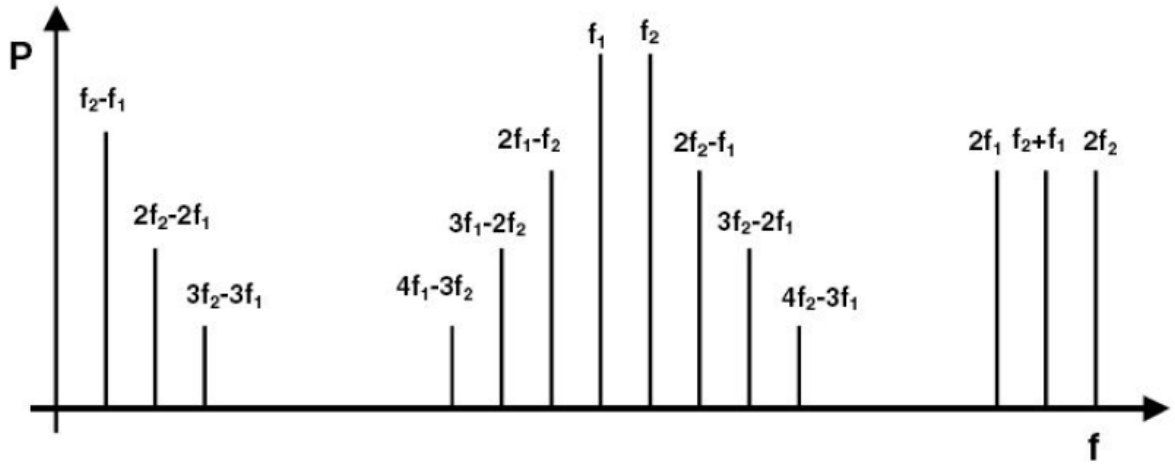

Figure 2.7 Intermodulation Distortion Frequency Spectrum

IMD frequencies are given by:

$$f_{IMD} = \pm n.f_1 \pm m.f_2 ,$$

Here, *n* and *m* are non-negative integers which sum to, *N*, the order of IMD (i.e., $N = n + m$). In theory, there will be many frequency combinations based on *n* and *m*, but in practice the magnitude of higher order products is less significant. As a result, typically focus is given on the lower order nonlinearities.

2.4.8 Receiver Blocking

An RF circuit can be approximated as a linear black box if all operating blocks are linear. This means that the small signal input receiver must be linear. However, for a high level input signal, the active components enter the nonlinear region and performance degrades. If the output of the circuit is a "compressive" or "saturating" function of the input, the gain of the amplifier is reduced. The 1-dB compression point can capture this. Similarly, the 3-dB compression point indicates the level at which the gain of an LNA is reduced by 3 dB. The OOB noise of the aggressor needs to be lower than the 3-dB compression point to avoid receiver saturation. This phenomenon is known as receiver blocking. For example, according to Bluetooth specifications [17], the 3-dB compression point of Bluetooth

radios needs to be -27 dBm for an interfering signal from 2484-3000 MHz. This band is adjacent to LTE B41, B7. Typically, a mobile phone in these bands transfers around 23 dBm. In theory, 4G signals in these specified bands need to be attenuated by over 60 dB before reaching the Bluetooth LNA. This is extremely difficult to achieve with state-of-the-art filtering in low profile handheld devices.

There are different ways to mitigate this issue. If LTE and Bluetooth use different antennas in the system, additional isolation can be gained from antenna to antenna isolation. If the combined isolation from the filter and antenna is not enough, the limits of the hardware have been reached. In that case, it is possible to further mitigate the interference using software in the time domain. The implementation of this approach depends on application and user cases. For example, in the Bluetooth-LTE scenario, often time domain multiplexing is used between LTE and Bluetooth to avoid simultaneous operation.

Figure 2.8 shows a typical response of a conventional surface acoustic wave filter response in the Bluetooth band [10].

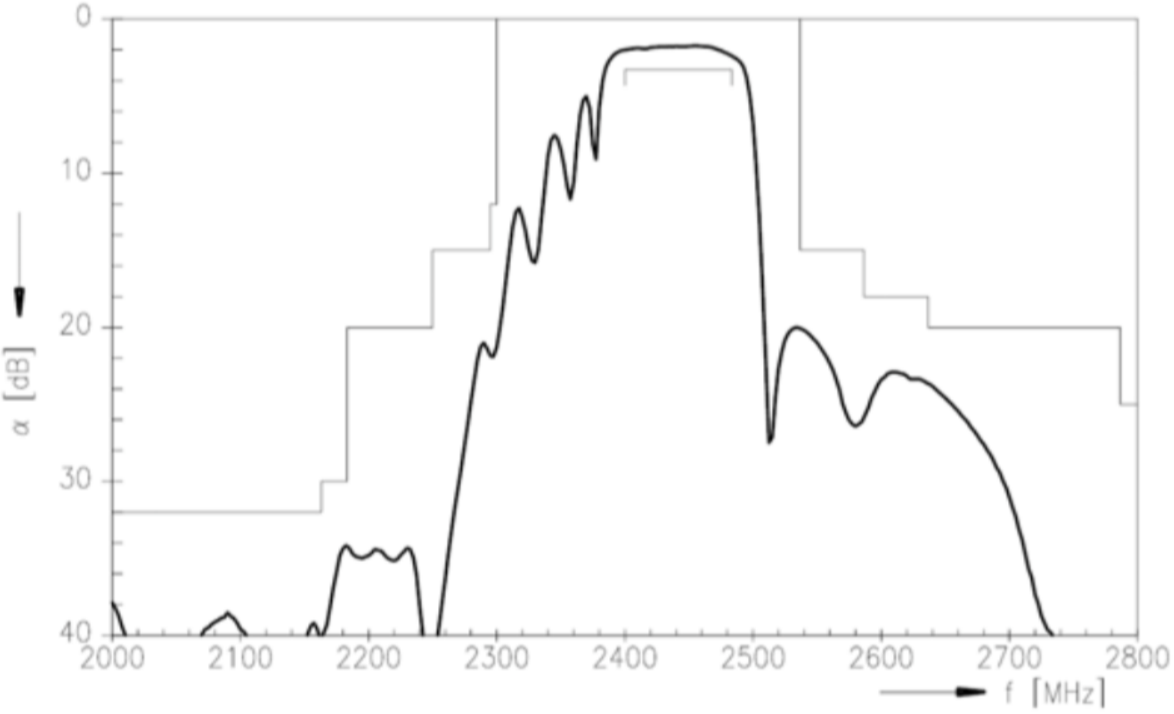

Figure 2.8 State-of-the-art Surface Acoustic Wave Filter Response

2.5 Passive Intermodulation

PIM means that the source of intermodulation or source of nonlinearity is passive. A passive device generally means a device that operates without external power. Examples of passive lumped elements are resistors, capacitors and inductors. In a typical radio system, passive components would include antennas, filters, couplers, isolators etc. On the other hand, active devices require external bias for activation. Basic building blocks of active devices are diodes and transistors. Any circuit that contains either a diode or a transistor is an active device. An active device could be an analog amplifier with a single transistor or a digital memory block with a million transistors. When designing, attempts are made to ensure that all active devices are able to operate in the linear region. When transistors operate in the active (linear) region, the small signal model is used for simulations. However, with a large signal input, active devices operate in the nonlinear region [18]. Passive devices, unlike active devices, are not expected to generate significant harmonics. However, under particular conditions discussed in this chapter, passive components can also exhibit nonlinear behavior. In typical user

cases, the impact of this is insignificant. For noise falling into the victim receiver bands, extremely low level of harmonics is acceptable, often in the range of -100 dBm. For a fundamental aggressor to be around 23 dBm (for cellular), this translates to over 120 dBc. This is a very low-level expectation. Due to the rapid proliferation of multiple radio coexistence systems, passive nonlinearity has become a significant design issue.

2.6 Mechanisms of Passive Intermodulation

Two types of mechanisms have been identified as leading to PIM [7]:

- Material Nonlinearity
- Contact Nonlinearity

2.6.1 Material Nonlinearity

Bulky materials, such as ferromagnetic materials exhibit non-linear I-V characteristics [7]. Magnetic hysteresis, for example, is a fundamental property of ferromagnetic materials. These materials, where permeability is a function of magnetic field intensity, exhibit a nonlinear response [19].

2.6.2 Contact Nonlinearity

The nonlinear I-V relationship of the metal-to-metal contact junction has been identified as one of the major sources of PIM. The actual mechanisms through which this action occurs are complex and not well understood. Studies have suggested the following explanations for these mechanisms [7]:

- Electron tunneling through thin oxide layers separating conductors at metallic contacts
- Micro discharges between micro cracks in metallic contacts
- Poor workmanship causing loose connections, metal cracks and oxidization at joints

In reality, it is likely that all of these factors combine together to cause PIM. This is one reason why it is very challenging to determine the exact contribution of each of these factors.

2.7 Electron Tunneling Through Metal-Metal Contact

Classical physics cannot explain tunneling. It is necessary to turn to quantum physics to understand the tunneling effect and why it is relevant to the discussion of PIM. Tunneling arose as an issue looking for an explanation, due to the development of modern electronic devices. In fact, electron tunneling is one of the major limitations of metal-oxide-semiconductor field effect transistor

(MOSFET) technology—a technology that forms the basic building blocks of every electronic gadget we see and use around us today [20].

The electron tunneling effect can be explained using Einstein's wave-particle duality theorem, a theorem that he used to explain the wave-like nature of light. Inspired by this, De Broglie proposed in his doctoral dissertation that matter can also be both particle and wave at the same time. He also proposed that there is an inverse relationship between the matter particle wavelength and the momentum of the particle. Heisenberg later elaborated on this with his uncertainty principle. The uncertainty principle states that the location of an electron and the momentum of an electron cannot be measured at the same time. The concept of position is therefore difficult for sub-atomic particles. An electron in orbit has no exact position at a particular time, rather it is somewhere in the orbit. Therefore, the quantum wave function concept came to be, which mathematically explains the superposition of associated quantum state at any particular moment. Instead of defining the position of particle, the probability of its state is described until measurement is done [21].

According to quantum physics, due to the wave like nature of an electron, there is a finite probability that an electron trapped behind a barrier may at times appear on the other side of the barrier [21].This phenomenon is called electron tunneling. A barrier basically means an energy delta between two states. This energy delta or barrier needs to be overcome for an electron to pass through. This phenomenon is illustrated in Figure 2.9 below.

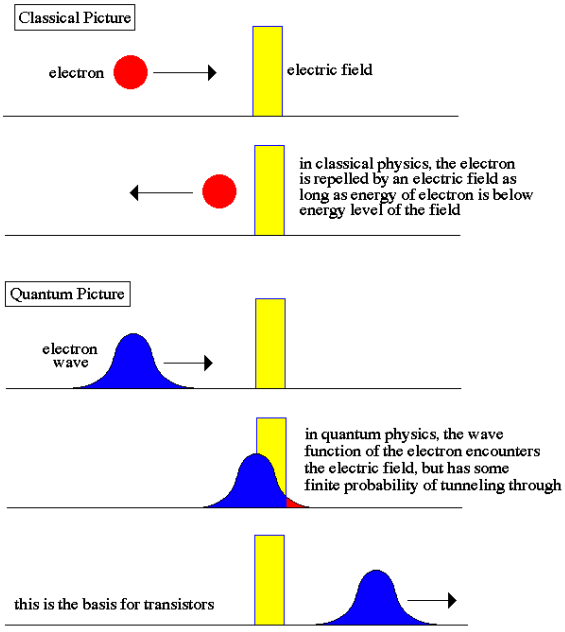

Figure 2.9 Electron Movement: Classical vs Modern Physics

A particle incident to the barrier can either be reflected or transmitted. The reflection coefficient (R) is defined as the ratio of the reflect-probability density to the incident-probability density. The ratio of the transmit probability density and incident-probability is defined as the transmission coefficient (T). The sum of these two probability densities has to be 1 [22].

$$T + R = 1$$

Finding T is necessary to find the electron-tunneling probability. If the potential energy of an electron is E, the barrier potential energy is U, the mass of the particle is m, h is Planck's constant, and the length of the barrier is L, then the transmission coefficient T for a square barrier can be calculated as [22]:

$$T(E) = \{1 + \frac{1}{4}\left[\frac{U^2}{E(U-E)}\right] sinh^2 \alpha L\}^{-1} \tag{2.6}$$

Where, $\alpha = \sqrt{2m(U-E)}/\hbar$

Looking at equation 2.6, it can be seen that the tunneling probability decreases if the length of the barrier increases. As the distance between the two contacts increases, the tunneling probability will decrease. Each metal-metal contact can potentially be a PIM source. In reality, there is no perfect metal-to-metal contact; all contact zones are actually separated by thin microscopic bumps and a thin dielectric layer. Hence the probability of a nonlinear current always exists [23]. Figure 2.10 shows a diagram of a contact model [23]. In this figure $\mathrm{R_t}$ represents the current constriction; $\mathrm{R_{const}}$ and $\mathrm{C_c}$ are the metal resistance and the metal capacitance, respectively; $\mathrm{R_{nlnc}}$ and $\mathrm{C_{nc}}$ represent the non-contact resistance and capacitance, respectively; and $\mathrm{R_{tv}}$ is the nonlinear current due to tunneling.

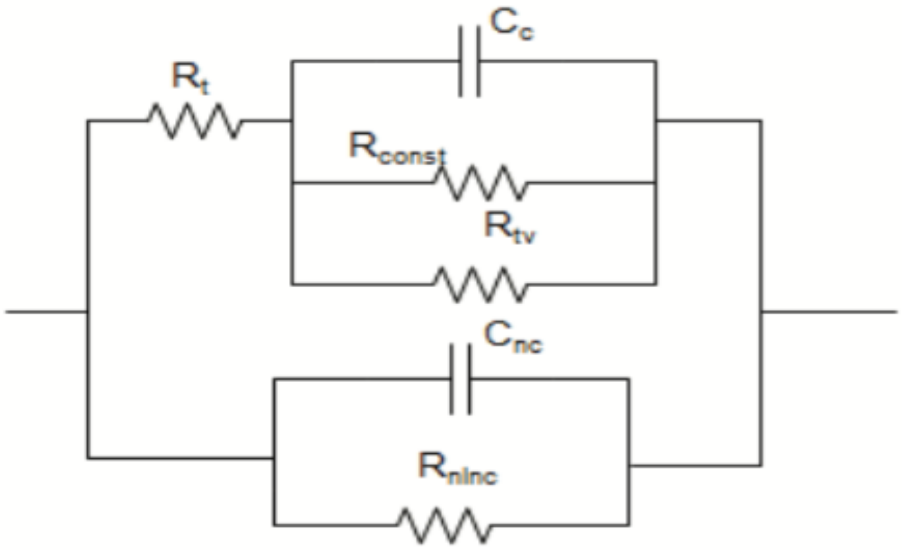

Figure 2.10 Simplified Lumped Model of Nonlinear Metal-Metal Junction

If V is the voltage between the two metal contacts, A_s is the contact area and J_{tv} is the nonlinear current density, then R_{tv} can be calculated as:

$$R_{tv} = V/A_s J_{tv}$$

The Simmons model is used to derive J_{tv}:

$$J_{tv} = \frac{e}{2\pi h s^2}\left[\varphi_0 e^{-4\pi\sqrt{\frac{2m\varphi_0}{h^2}}s} - (\varphi_0 + eV)e^{-4\pi\sqrt{\frac{2m(\varphi_0+eV)}{h^2}}}\right] \quad (2.7)$$

Where φ_0 is the work function of the particle material, and s is the dielectric thickness.

2.8 Low Profile Mobile Antennas

From the above discussion, a few key points should be emphasized. Tunneling depends on the metal-to-metal distance in the junction, the material work function and the size of the contact area etc. Since the focus of this thesis is the nonlinearity that is directly caused by the antenna system, it is critical to identify the areas of the antenna structure where current density is high. A higher input level facilitates the electrons' ability to gather enough potential energy to cross the barrier. To analyze the potential sources of nonlinearity, it is therefore important to understand the current density of the radiating structure. One of the most widely used low-profile antennas is the planer inverted F antenna (PIFA). Below a brief study is presented in which potential high current density areas are located. Here, a PIFA is being used as an example case, in reality different antennas have different patterns. The current density pattern depends on the system housing, material, resonance, bandwidth etc. Often screws, pogo pins, conductive fabrics are used for contact between two metal parts [24]. These can become potential sources of nonlinearity, because of the discontinuity of the structure. In addition, due to system constraints, proper grounding cannot always be guaranteed.

2.8.1 Planer Inverted F Antenna

PIFAs are commonly used for cellular phones. Their ease of fabrication, low cost, low profile and simple structure have made them popular antennas for handheld portable devices [25]. Figure 2.11 shows a typical PIFA design and its associated dimensional and structural parameters [26]. Its resonance depends on L1, L2, W and H. The planar element, parallel to the ground plane, is responsible for radiation. The resonating length should be equal to the half wavelength of the resonance frequency. The current is at its maximum at the shorting location. The feed is positioned in a way so that maximum power is transferred to the antenna from the radio-conducted port [27]. One of the points of interest is that the dimension of the ground plane is critical to the efficiency of the antenna [28].

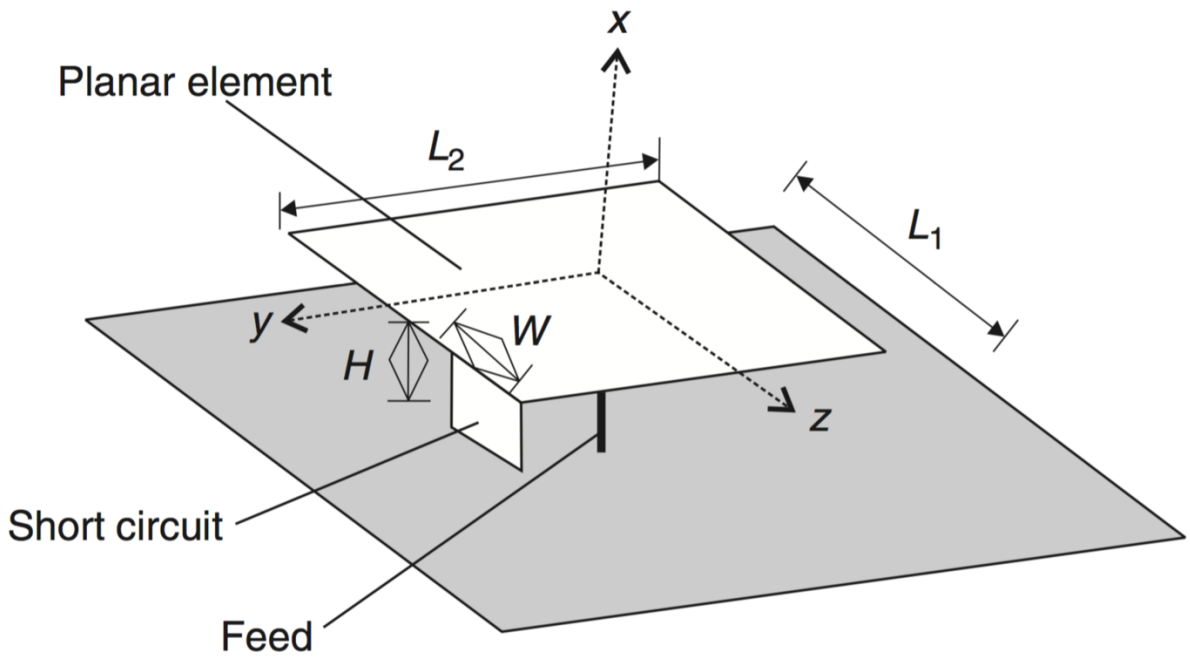

Figure 2.11 Planer Inverted F Antenna Diagram

In a cell phone, the ground plane is typically the housing. The actual wavelength of the radiator depends on the material's properties and dielectric constant. The dielectric material slows down the wave's velocity but does not affect the wave frequency. As a result, the effective wavelength becomes smaller than the free space wavelength. To calculate the length of a PIFA planar element for a cellular low band (800 MHz), equation 2.8 is used. Here C is the speed of light in free space, f is the operating frequency and λ is the wavelength.

$$C = f \times \lambda \tag{2.8}$$

For 800 MHz, the free space full wavelength is calculated as:

$$\begin{aligned} &\lambda = C/f \\ &\text{Or, } \lambda = (3 \times 10^8)/(800 \times 10^6)\ \text{m} \\ &\text{Or, } \lambda = 37.5\ cm \\ &\therefore Quarter\ Wavelength\ , \frac{\lambda}{4} = 9.375\ cm \end{aligned} \tag{2.9}$$

This calculation suggests that the length of the resonator and the length of the ground plane in free space need to be roughly 9 cm. The actual length needed will be smaller because inside the cell phone

there will not be free space, but instead a complex dielectric constant. The effective wavelength, λ_d is calculated as:

$$\lambda_d = \frac{\lambda_{free\ space}}{\sqrt{\epsilon_r}} \ , \tag{2.10}$$

Here ϵ_r is relative dielectric constant of the material.

As the interior of the cell phone is not in free space, the final effective quarter wavelength needed is actually somewhere between 5 to 8 cm. This indicates that the full dimension of the cell phone will be required to construct the antenna. Table 2.1 shows the dimensions of a few popular cell phones [24].

Table 2-1 Antenna Types and Dimensions of Different Mobile Phones

Model	Antenna Type	Length, mm (Largest Dimension)	Band
Sony Ericsson Z600	PIFA	43.6	GSM900, 1800,1900
Nokia E60	PIFA	40.0	GSM900, 1800,1900 + 3G
Motorola W208	PIFA	35.6	GSM900, 1800
BlackBerry 8100	Planar Monopole	42.0	GSM850/900/1800/1900
iPhone 4	Planar Monopole	58.0	GSM850/900/1800/1900+3G

The visible slot or flex on the unit is used as part of the antenna. The full housing is often used as the radiator. This means that the critical contact can be anywhere in the housing. The exact location is dependent primarily on the current density and radiation pattern.

2.8.2 Design in Existing Products

The current density of the antenna depends on the type of antenna being used. Figure 2.12 shows the current distribution and three-dimensional radiation pattern of a PIFA (1.8 GHz) used in the Motorola T193 cell phone [24].

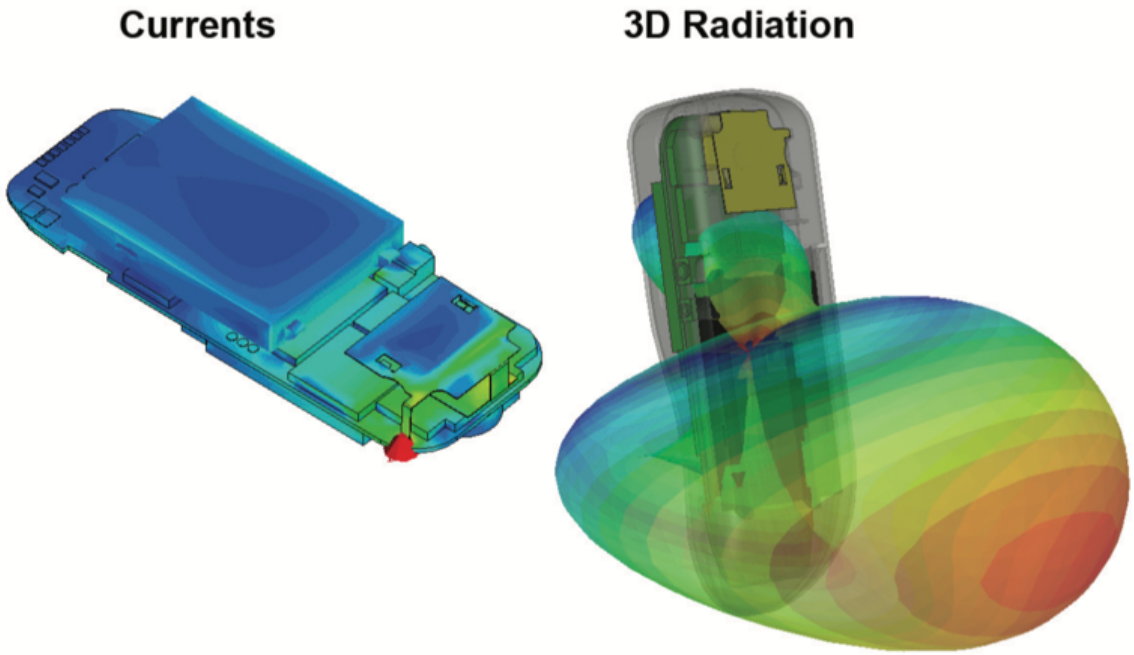

Figure 2.12 PIFA Current Distribution in a Motorola T193

The current density is highest around the antenna, and lowest around the motherboard and the rest of the housing. Far field radiation is also dominant upward from the antenna. A small amount of leakage downward is due to the finite ground area. There is also a high current density at the feed and the shorting pin.

Figure 2.13 shows the current distribution of a planar monopole antenna (1.9GHz) used in the iPhone 3 and iPhone 4 [24]. In both cases the current density is highest near the feed and ground.

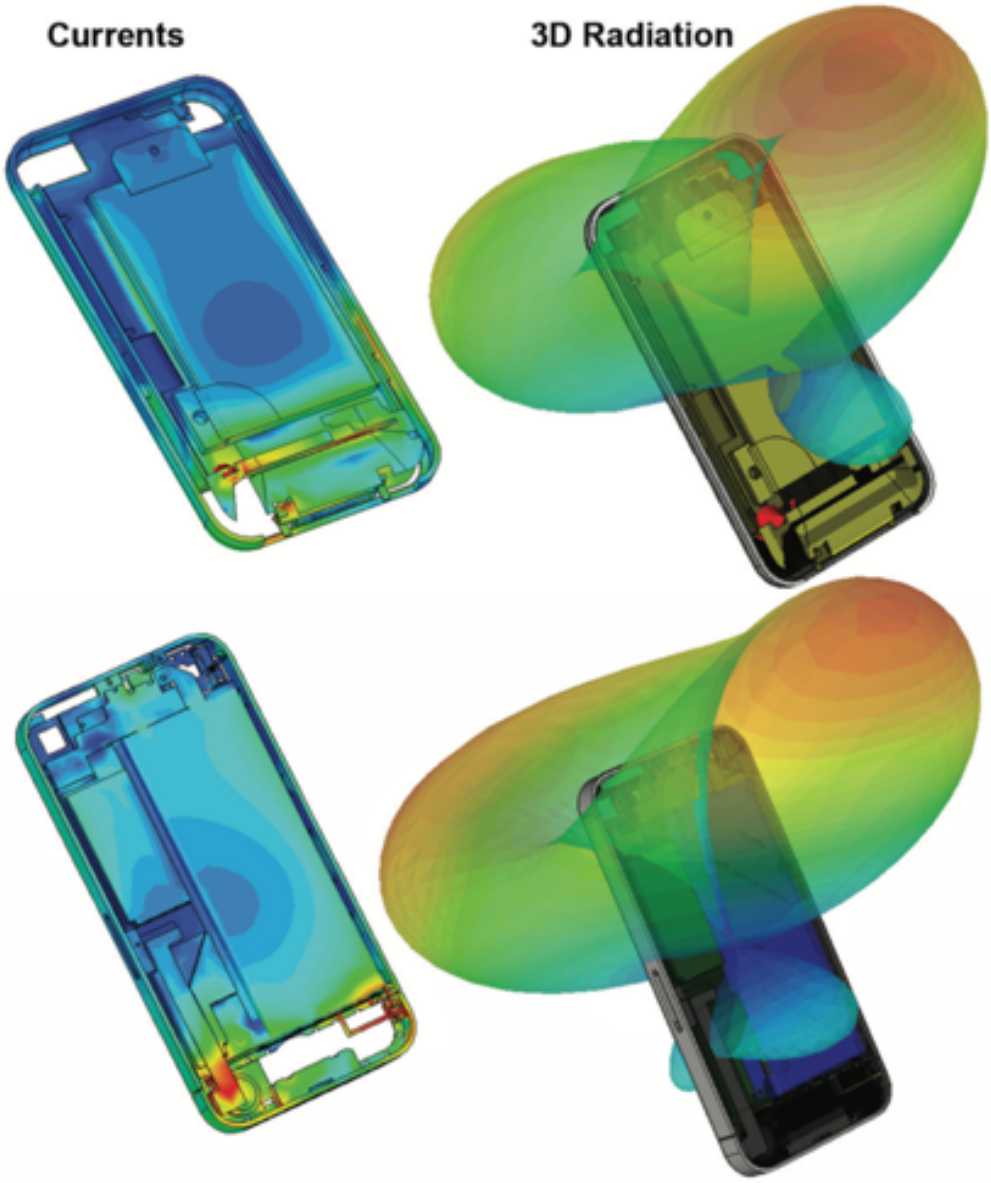

Figure 2.13 Current Distribution of iPhone 3 (top) and iPhone 4 (bottom)

Due to the high current density at these locations, the contact mechanism used at the ground pin and feed is very critical for the antenna's performance. For practical mechanical reasons, all of these contacts cannot be soldered. Often pogo pins or spring connectors are used for the antenna-element-to-ground-plane contact and the motherboard-to-feed launch.

Figure 2.14 shows the Nokia 8850's dimensions (in mm) [24]. In order to improve its radiation efficiency, Nokia extended the ground plane and connected the motherboard ground plane through a pogo pin.

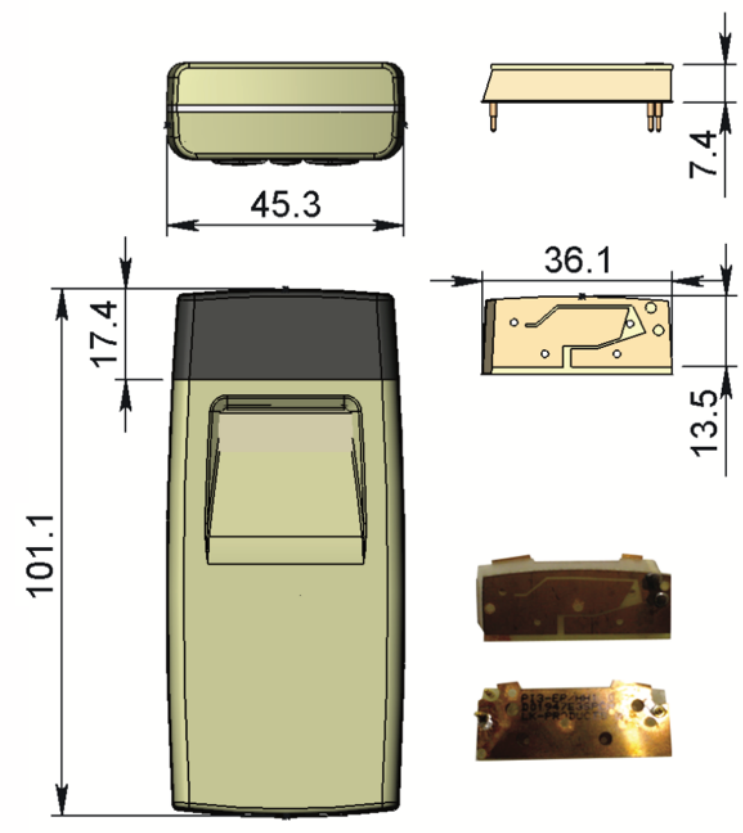

Figure 2.14 Nokia 8850 Ground Connection Through Pogo Pin

In Figure 2.15, the Samsung Galaxy Note's antenna is shown. The antenna is launched to the motherboard through a spring connector [29].

Figure 2.15 Samsung Galaxy Antenna Launch Through Spring Connector

Similarly, in the BlackBerry 9000, critical contacts are made using spring type connectors as shown in Figure 2.16 [30].

Figure 2.16 BlackBerry 9000 Critical Contact

The BlackBerry uses pogo-pins and spring connectors in its antenna designs. Different applications require different feed designs, ground shorting pin designs and varying housing extensions to accommodate a larger ground surface. Since current density levels are hot in these interfaces, these areas need special attention.

Metal-to-metal junctions are a nonlinear source that can cause PIM. The probability of PIM increases significantly at junctions that are at a current hotspot.

Chapter 3
Development of Measurement Test-bed and Fixture

In order to understand the causes of intermodulation generation, component level measurement is required. Any passive component is a potential suspect. To conduct component level measurements, a well-designed and robust test fixture and measurement setup that meets strict measurement requirements is necessary. The precise design of both the test fixture and measurement setup is key to accurately characterizing and analyzing PIM performance, particularly if the design goal is to improve receiver sensitivity.

In this thesis, the investigative goal is to measure intermodulation generated by the antenna connector. In this chapter, three distinct topics are covered to describe the experiment and equipment:

- Device (antenna contact) under test
- Reference design for setup validation
- Test fixture development

3.1 Antenna Contact Under Test

3.1.1 Design Considerations

In any device, there are plenty of suspect sources of nonlinearity. In order to isolate and quantify individual contributions, it is necessary to design an antenna contact under test (ACUT) that will closely mimic the actual cell phone operating environment. Unlike other passive components such as filters and couplers, prototyping an antenna connector on a fixture is a design challenge. A number of things were taken into account in order to carefully design the fixture. These considerations are summarized below.

The probability of PIM generation is maximized if the current density flowing through the suspect component is high. Since nonlinear junctions cause PIM, controlling the amount of current that flows through the junction is critical. The linearity/nonlinearity of the junction determines whether or not the device operates in the linear/nonlinear region. As discussed before, contacts located at the feed or at any non-distributed narrow ground path carry the highest amount of RF current.

An antenna is a passive component by design in most cases. In a perfect, no-loss world, an antenna would deliver all the power that is input to its feed. In reality this never happens. The ratio between

the radiated power and input power is called the antenna efficiency [31]. To maximize antenna efficiency, it is important to have a large ground area. Antenna radiation volume is also critical for efficiency; in general, higher volume is better. The amount of power that is input to the antenna is also very critical. Finally, the feed needs to be matched to the antenna for maximum power transfer from radio to antenna.

The target was to prototype the antenna connector. Typically, a transmission line is designed to carry the input signal to the antenna feed. This transmission line can be a microstrip line or coaxial cable. One side of the cable is connected to the radio and the second side is connected to some launch mechanism that connects to the antenna. As discussed in Chapter Four, different types of connectors, including pogo pins and spring connectors, can be used for this purpose. This connector is also used as an antenna-ground-to-system ground contact as well. For this thesis, the goal was to mock up an experimental metal-to-metal contact. To do this, a spring connector was selected to emulate the metal-to-metal contact.

This prototype does not truly represent an antenna as the goal here is not to analyze the antenna performance. The prototype was designed so that a critical contact in an antenna system could be emulated. The exact location of this critical contact will vary from antenna to antenna as discussed in the preceding chapter.

3.1.2 Feed and Antenna Contact

In order to make sure that maximum power is transmitted to the antenna, the feed system needs to be matched with the radio conducted RF port. A conducted RF port is by convention matched to 50-ohms. Therefore, the antenna feed system needs to have an impedance that is close to 50-ohm as well. In order to achieve this, a 50-ohm microstrip line was designed on a FR4 printed circuit board (PCB). FR4 is the most popular PCB material for mobile phones [32]. The antenna connector is typically soldered on the feed side and makes a pressure-based contact with the antenna. To simulate this junction, at the centre of the line a discontinuity was added and an antenna connector was soldered.

To mimic the antenna contact, another piece of metal on FR4 was designed and placed on top of the connector. To simulate real-world conditions, pressure needs to be applied on top of this piece. Again, the purpose of this experiment is not to design an efficient antenna, but instead to design an antenna contact interface. Ideally, the second metal piece would radiate if this were an exact duplication of an actual antenna contact. However, this would add complexity to the measurement as

it would require a radiated measurement to be performed. In order to be able to measure both reflected and forward PIM noise, the decision was made to design for a conducted measurement. Therefore, a symmetric design was implemented with a second connector, which also made contact with the interface. This arrangement means that a forward and reverse path exists which facilitates conducted measurement. This is illustrated below in Figure 3.1, which shows a computer-aided design (CAD) model of the prototype feed line and connector. In the figure, it can be seen that the top metal mimics the antenna while the bottom trace mimics the feed line.

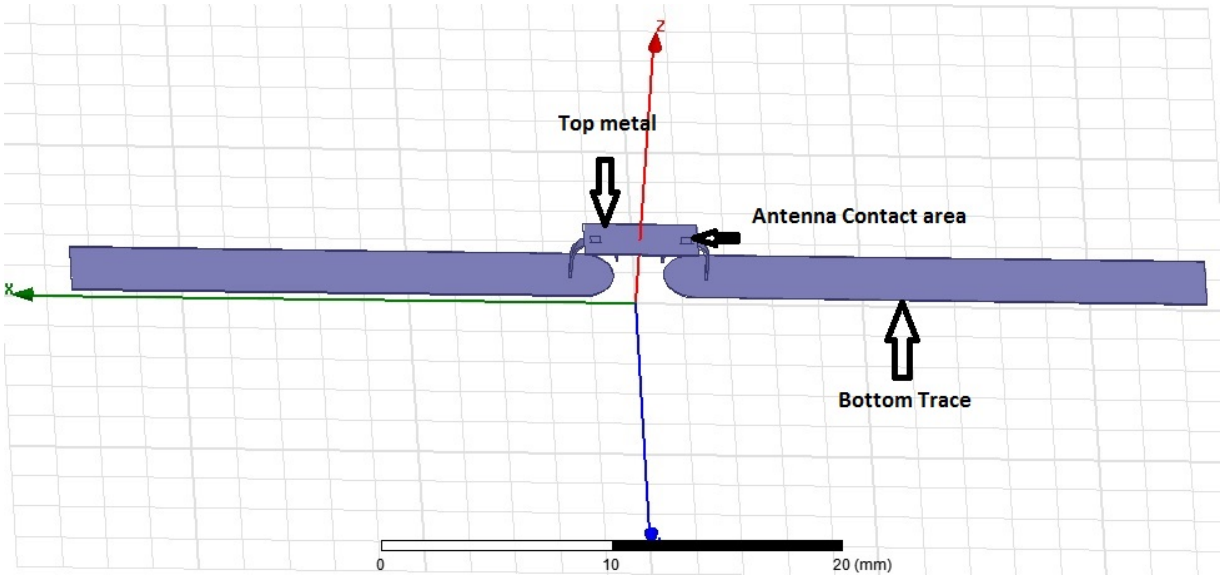

Figure 3.1 Prototype CAD Model of Connector and Contact Surface

A discontinuity at the center of the microstrip line contributes to impedance mismatch. This mismatch can potentially change the characteristic impedance of the contact system. To compensate for this mismatch, the gap between the two sides of the line was optimized. The design target was to ensure that the linear performance of the connector system is the same as the linear performance of the microstrip line when there is no discontinuity. The length and width of the top metal were also optimized. The effect of fixture material was also considered during the optimization. The ANSYS HFSS package was used for full wave simulation to optimize the test kit. Figure 3.2 below shows the parameters that were optimized.

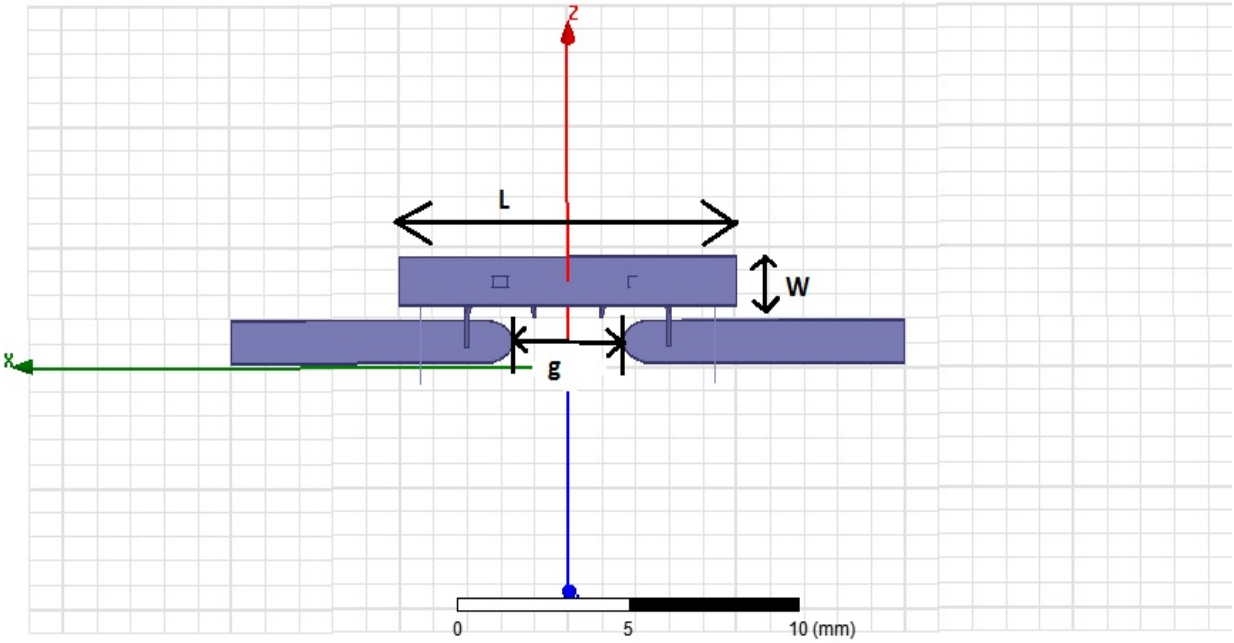

Figure 3.2 Variable Parameters of Optimized ACUT

The final dimensions after test sample optimization are shown in the following figures. Figure 3.3 points out the gap distance, the thickness of the FR4 material and the width of the trace. Figure 3.4 shows the top metal dimension. Figure 3.5 shows the return loss and insertion loss of the final test kit. Insertion loss and return loss are reasonably matched for a 50-ohm system.

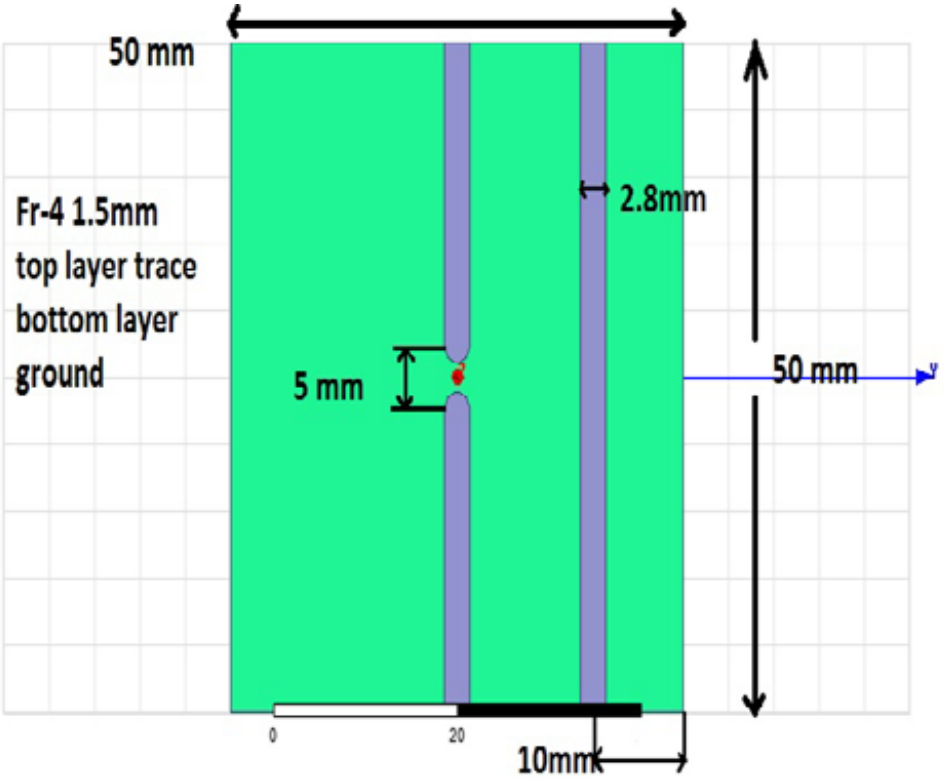

Figure 3.3 ACUT Design Parameter: Gap Between Discontinuity

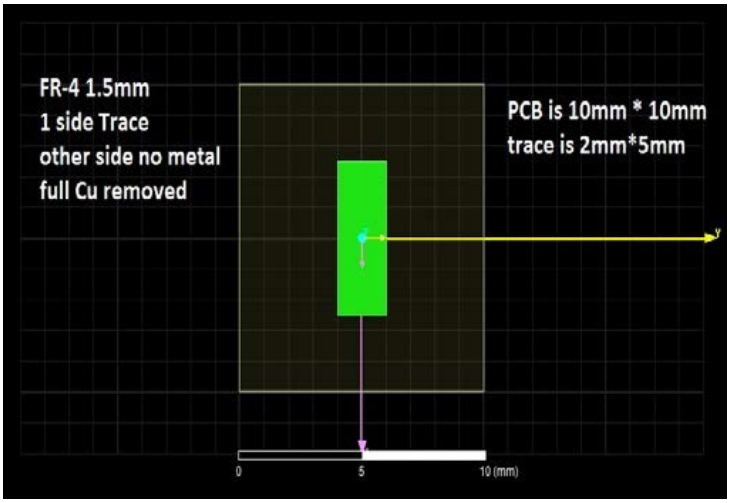

Figure 3.4 ACUT Design Parameter: Top Metal Thickness

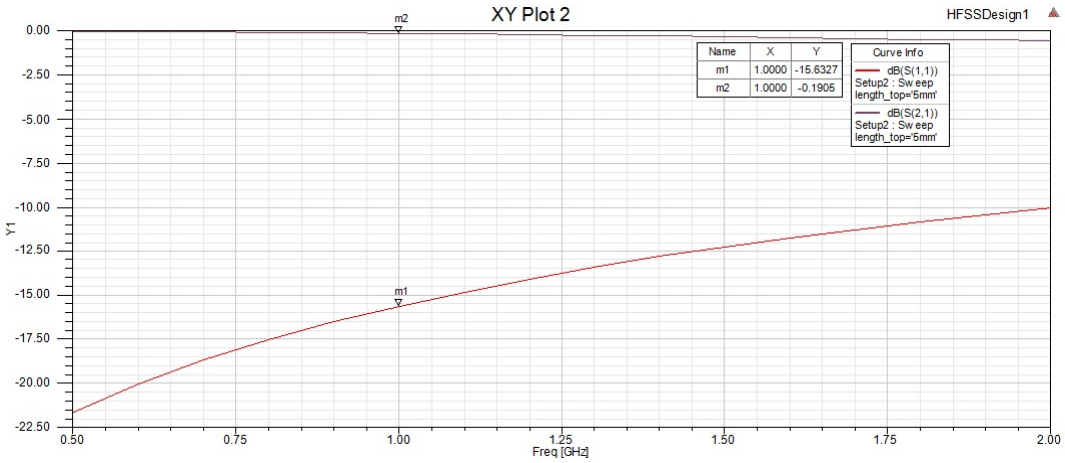

Figure 3.5 ACUT Linear Response

3.2 Reference Design for Setup Validation

Designing a baseline kit is extremely important in order to accurately validate the setup. As mentioned before, the biggest challenge to PIM measurement is the design of a setup that does not generate PIM. The only way to confirm that the setup is clean, is to design a baseline reference to measure system response.

A baseline microstrip line on the same FR4 board was designed for contact measurement. This microstrip has the same specification as the primary test sample. Figure 3.3 above shows the experimental test sample and the baseline test sample on the same board. In the baseline sample, there is no discontinuity; it is a simple 50-ohm microstrip line. This allowed for a way to determine the quality of the measurement system and how it would affect the accuracy of the measurements taken from the metal-to-metal contact.

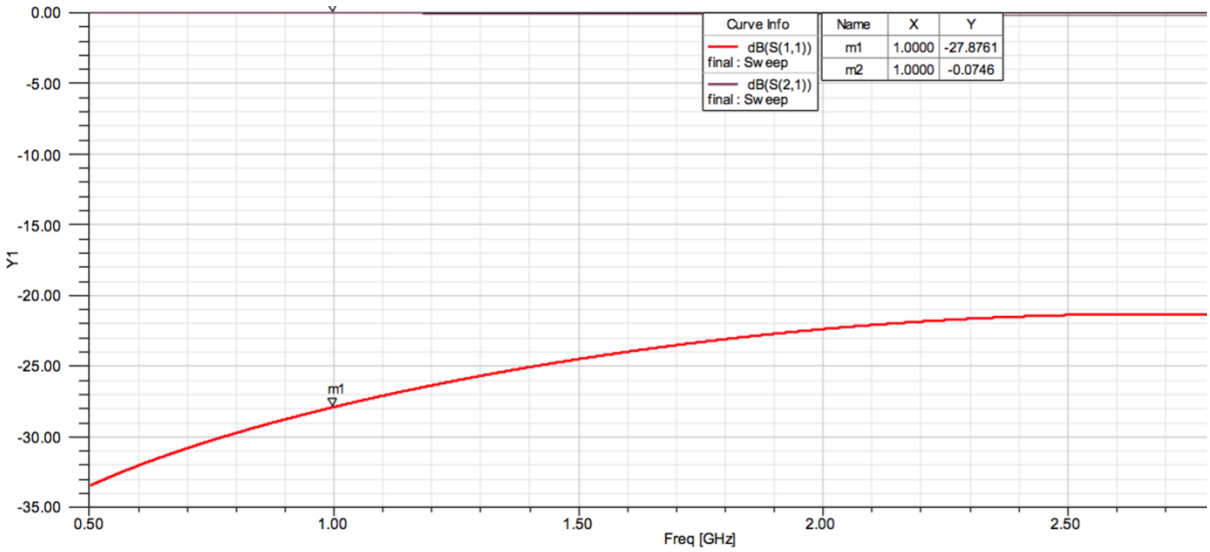

Figure 3.6 Linear Response of Baseline Design

3.3 Test Fixture

Figure 3.7 shows a side view of the contact system with the fixture.

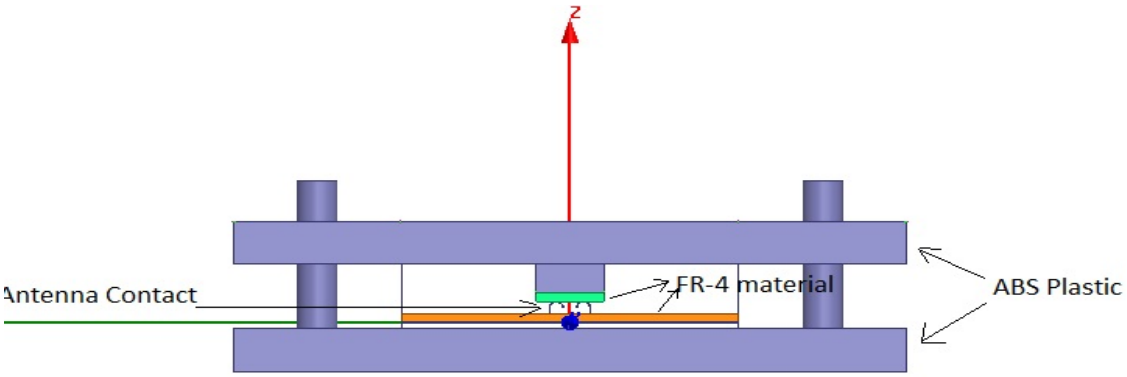

Figure 3.7 Side View of Contact System

In order to obtain repeatable and meaningful data, a support structure was also designed. This structure was constructed with acrylonitrile butadiene styrene (ABS) plastic material. This structure was designed symmetrically across the center of the microstrip line.

It was very important to make sure that equal pressure had been mounted on top of both connectors. To achieve this goal, two separate parts were designed: a bottom part used to hold the PCB with microstrip line (mimics the feed with connector), and a top part used to hold the PCB with the antenna representation. In order to align the bottom and top parts, four cylindrical poles were designed. The poles were designed with a smooth surface to reduce friction between the top part and the poles. The idea of the pole is to ensure seamless vertical movement of the top structure and to limit horizontal movement. Figure 3.8 illustrates a top tilted view of the fixture and contact system.

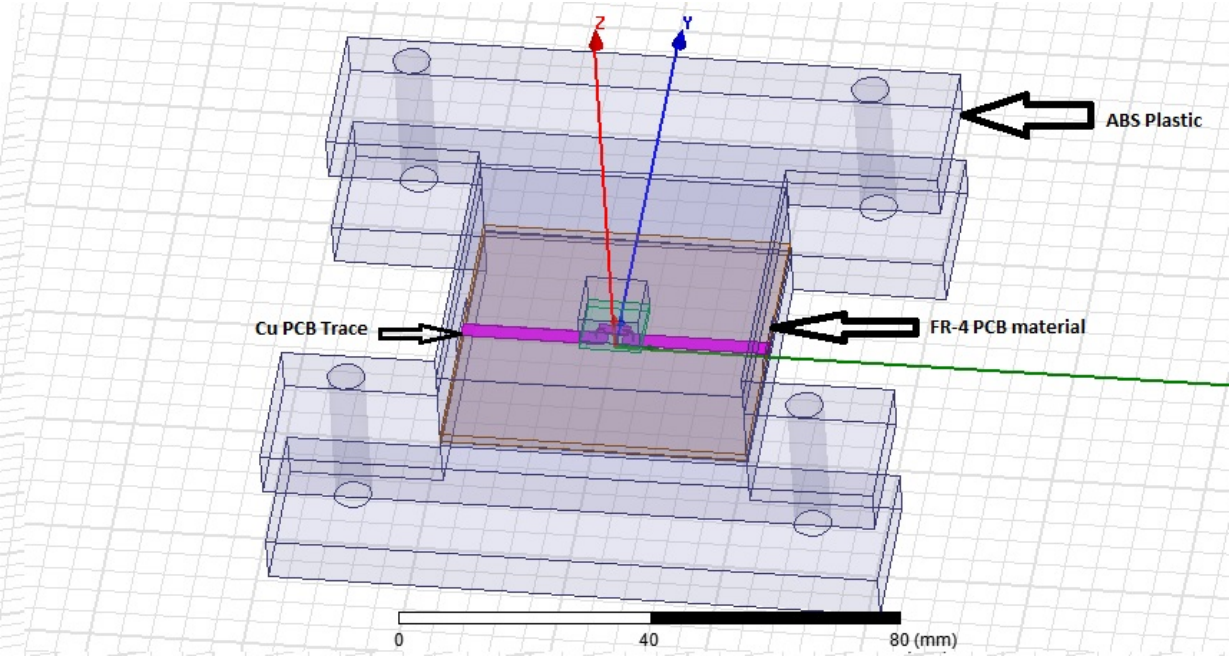

Figure 3.8 Top Tilted View of the Contact System

Chapter 4
Test Setup and Experimental Results

An IMD measurement setup must always be carefully designed, but especially so for a receiver design. This is due to the low level of the desired noise floor required for receiver designs. For the setup for this thesis, the following designs considerations were examined:

- Desired frequency of operation would fit into the United States' Cellular Band
- Test setup to be as realistic as possible given availability of high quality RF filters

4.1 Frequency Selection

For this experiment, a 2-tone IMD test setup was designed to measure 3rd order nonlinearity. The two tones are identified as f_1 and f_2. The frequencies are given below:

$f_1 = 824.6\ MHz$

$f_2 = 848.0\ MHz$

$IMD = 2 * f_2 - f_1$

$IMD = 871.4\ MHz$

The frequencies were selected intentionally to fall within the United States' Cellular Band. The main reason for choosing these frequencies was a direct result of the availability of high quality duplexers for the transmit (Tx) and receive (Rx) bands. The duplexer is a primary component for IMD measurement (discussed later in this chapter).

4.2 Test Equipment

Below is a list of the test equipment used in this experiment:

- Spectrum Analyzer (Agilent PXA with Pre-amplifier)
- Signal Generator (Agilent ESG)
- Class A Power Amplifier (Mini-Circuits Lab)
- Cellular Duplexer
- RF Isolator

- RF Combiner
- RF Directional Coupler
- Cellular Rx Band Pass Filter (BPF)

The measurement setup schematic is shown in Figure 4.1.

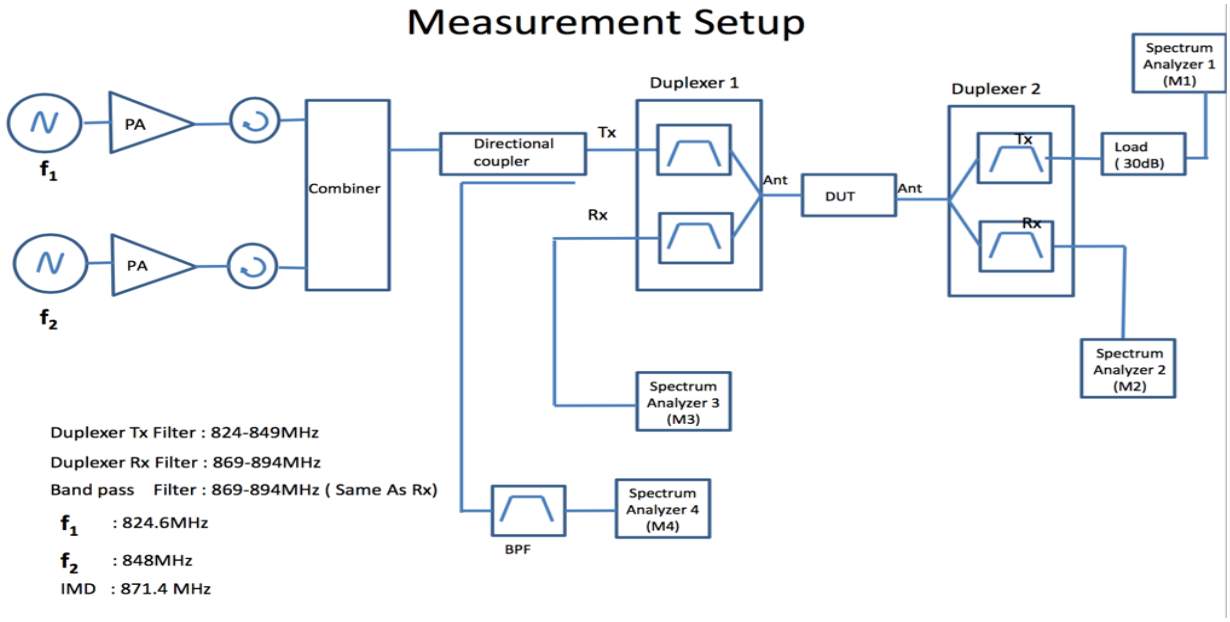

Figure 4.1 Measurement Setup Schematic

A photograph of the complete test set up is shown in Figure 4.2.

Figure 4.2 Actual Measurement Test Setup

4.3 Relevance of Setup Equipment

Technically, since this is a 2-tone test, two signal generators are required. Since the ACUT has a one port input and a one port output, a combiner is needed for the input port. Given that the goal is to measure the IMD spectrum, a spectrum analyzer is needed. Typically, a single spectrum analyzer would constitute the test setup, however, because of other concerns, additional circuits and equipment are required.

4.3.1 Addition of Power Amplifier

For real-world applications, the cellular transmit power is typically between 23-25 dBm for LTE, 33 dBm for GSM cellular and 30 dBm for PCS bands [38]. For this experiment, 25 dBm was selected as the fundamental transmit power level. As the fundamental power increases, the IMD only gets worse. However, the filtering acquired for the setup (given financial resource considerations) meant that noise levels for powers higher than 25 dBm could not be handled. Available signal generators could transmit to a maximum of 5 dBm, therefore, a power amplifier was added to reach 25 dBm. The experiment used a class A power amplifier from Mini-Circuits Lab with a 3 W output capability. Class A was chosen due to the strict linearity criteria required of the test setup.

4.3.2 Addition of Isolator

Port-to-port isolation of the combiner is typically around 25-30 dB [33]. This results in a 0 dBm power level at the power amplifier frontend from f_1 to f_2 and vice versa. This level might damage the power amplifier and compromise the linearity performance. In order to avoid this two isolators were used, one at the output of each amplifier. Isolators are 2-port networks that let power flow in one direction but block power flow in the reverse direction.

4.3.3 Addition of Duplexer (Duplexer 1)

In order to ensure that the ACUT has a clean fundamental signal input, a duplexer is needed. A clean fundamental signal will prevent any receiver sensitivity degradation. The setup currently consists of two signal generators, two power amplifiers, isolators, a combiner and cables. Before the combined signal enters the ACUT, the ACUT input spectrum must be free from IMD tone. In order to ensure that this was so, a cellular duplexer was used. A duplexer common port was connected to the ACUT input. The Tx port was connected to the combiner side. The reason it was done this way, was to enable the measurement of the reflected IMD from the ACUT. The duplexer Rx port was used to measure the reflected IMD.

4.3.4 Addition of Coupler

In order to measure how much IMD the setup generated, a coupler was added between the combiner and the duplexer. The coupler input was connected to the combiner output and its output was connected to the duplexer Tx port. The coupled port was used to measure the IMD level via a spectrum analyzer.

4.3.5 Addition of Band Pass Filter

To ensure a clean measurement, a band pass filter was also used. The coupler coupled port contains both fundamental signals and all nonlinear products. Typically, a spectrum analyzer will generate nonlinear products at a signal level above 10 dBm [15]. Since the input signal used was much higher than that level, the spectrum analyzer at this power level would generate significant IMD. In order to avoid this, a band pass filter was used. The filter used a passband that was the same as a cellular band's Rx passband. This allowed the measurement of the actual IMD product generated from the antenna contacts and not from the spectrum analyzer.

4.3.6 Addition of Duplexer (Duplexer 2)

Once 2-tone fundamental signals enter the ACUT, IMD can be generated in both the forward and reverse directions. Reflected IMD was measured through Duplexer 1. To measure forward IMD, a second duplexer was needed, Duplexer 2. The duplexer common port was connected to the ACUT output. The Rx port was used to measure forward IMD. The Tx port was used to measure fundamental power. It is very critical to make sure fundamental power is normal during measurements. If fundamental power is low, then the measurement will not be valid. In this way it can be confirmed that the connector is not broken. A power sensor is basically a diode detector at the front end [34]. Power sensors can generate a high level of nonlinear products. In order to prevent the power sensor from generating nonlinear products, a 30 dB attenuator was placed at the power sensor's input.

4.4 System Level Simulation

In order to confirm the system's linear response was within an acceptable range, a system level simulation was run. Keysight's (formerly known as Agilent) ADS package was used for simulation. Each individual part's S-parameter was measured and added to the simulation model. The S-parameter is a linear simulation; however, the purpose of conducting this simulation is not to quantify nonlinearity. It is to make sure that the setup includes adequate filtering to prevent the spectrum analyzer from generating harmonics. Figure 4.3 shows the schematic of the model and ports of which the isolations have been measured.

Figure 4.4 indicates the insertion loss between the source and receiver. According to Figure 4.4, the insertion loss between the input and spectrum analyzer is 171 dB at f_1 and 149 dB at f_2. Assuming a 25 dBm input power level, the powers that will reach the spectrum analyzer are calculated below:

- Tone level at the reverse path (port 4):
    - At 825 MHz = 25 – 171 = -146 dBm
    - At 848 MHz = 25-149 = -124 dBm
- Tone level at the forward path (port 3):
    - At 825 MHz = -150 dBm, at 848 MHz = -124 dBm

The calculated levels above would not load the spectrum analyzer.

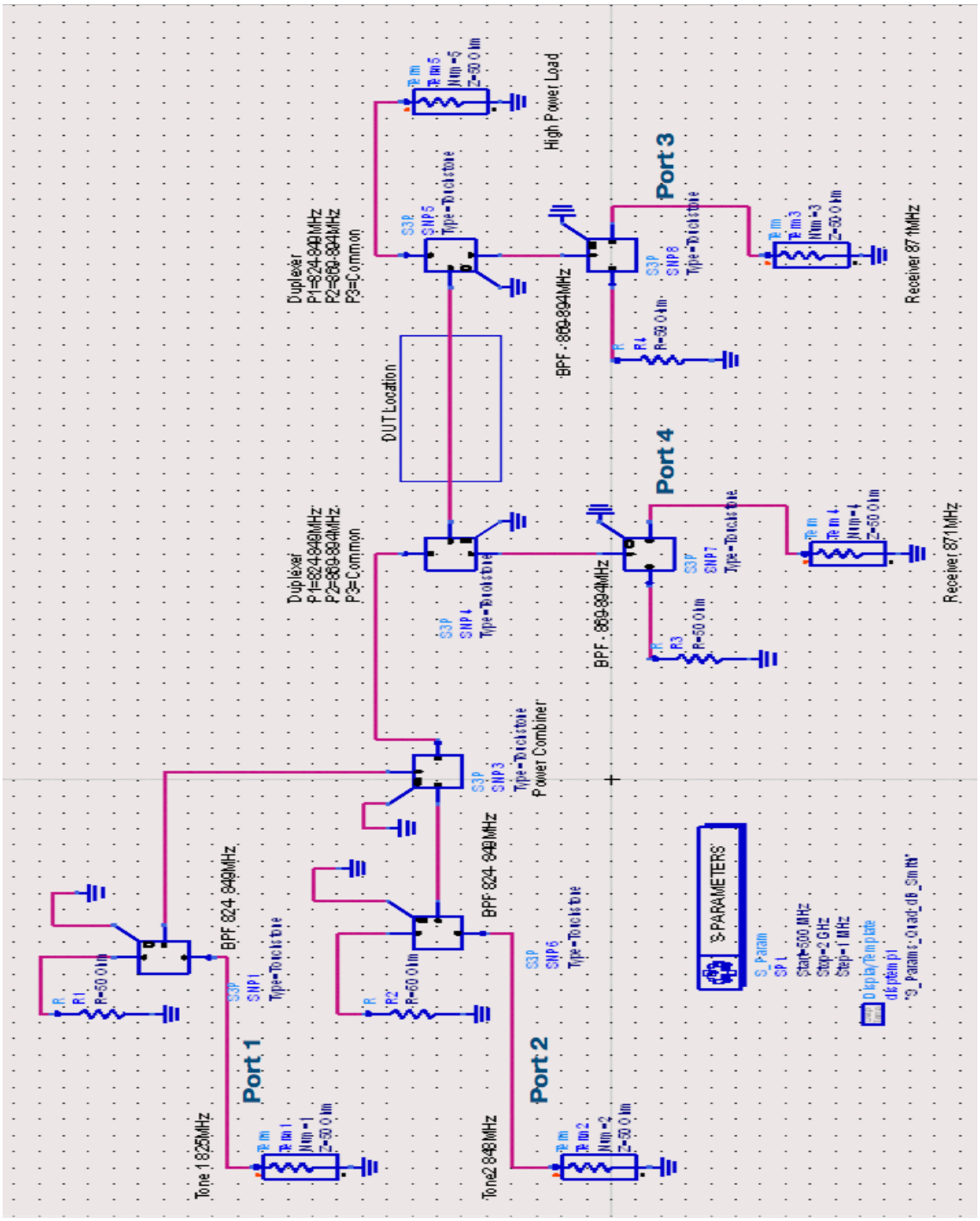

Figure 4.3 Linear Parameter Measurement Setup Schematic

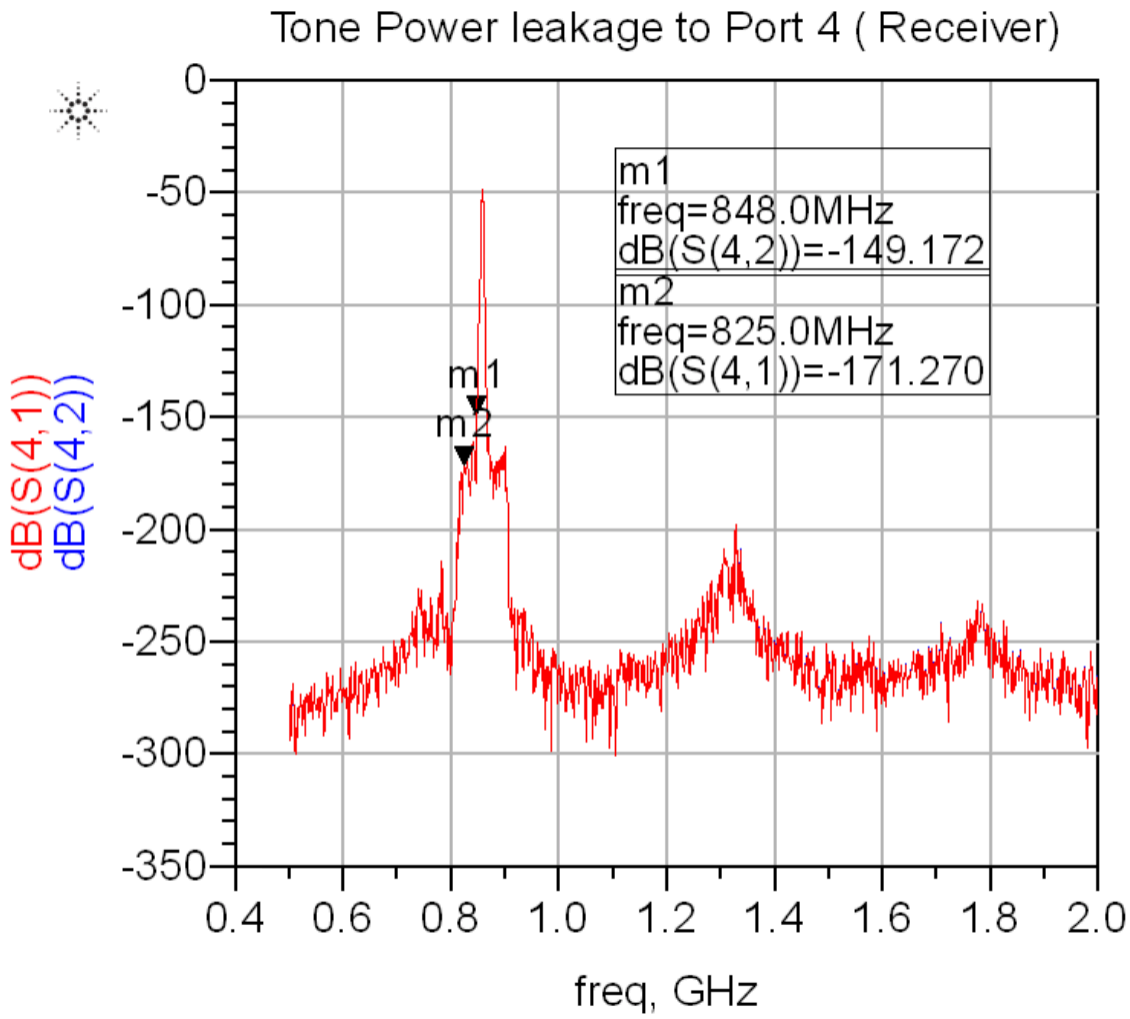

Figure 4.4 Insertion Loss between Source and Receiver

4.5 Test Procedure

Once the simulation was completed, the basic link budget of the setup confirmed its dynamic range. The following steps were carried out to conduct the measurements (refer to Figure 4.1).

- The ACUT was assembled and its S-parameters were measured with a vector network analyzer (VNA).

- All cables and connectors were cleaned with isopropyl alcohol to reduce system level nonlinearity. The setup was wired without the ACUT.
- Individual tone levels were adjusted to obtain a 24 dBm level at the input ACUT by measuring the spectrum analyzer at M1.
- Two spectrum analyzers were used simultaneously for the experiments. One was positioned at M1 and the other was used at various measurement points (M2, M3, M4). All other unused measurement points were terminated with a 50 ohm matched load. The purpose of keeping M1 monitored at all times was to confirm that the link did not break during the measurement.
- Baseline IMD level measurements were obtained at measurement ports without the ACUT.
  - Forward IMD (M2)
  - Reflected IMD (M3)
- The ACUT was added to the setup and measurements were taken from all ports.
  - Power at load (M1)
  - Forward IMD (M2)
  - Reflected IMD (M3)
  - Residual IMD from setup just before duplexer 1 (M4)
- All measurements were done in a shielded room to avoid external signal coupling to the setup and especially to the ACUT.

4.6 Measurement Results

4.6.1 Linear Response

Figure 4.5 below shows the return loss and Figure 4.6 shows the insertion loss of the ACUT. The return loss is measured to be better than 20 dB at the frequencies of interest. The insertion loss is 0.3 dB at the IMD frequency (871 MHz).

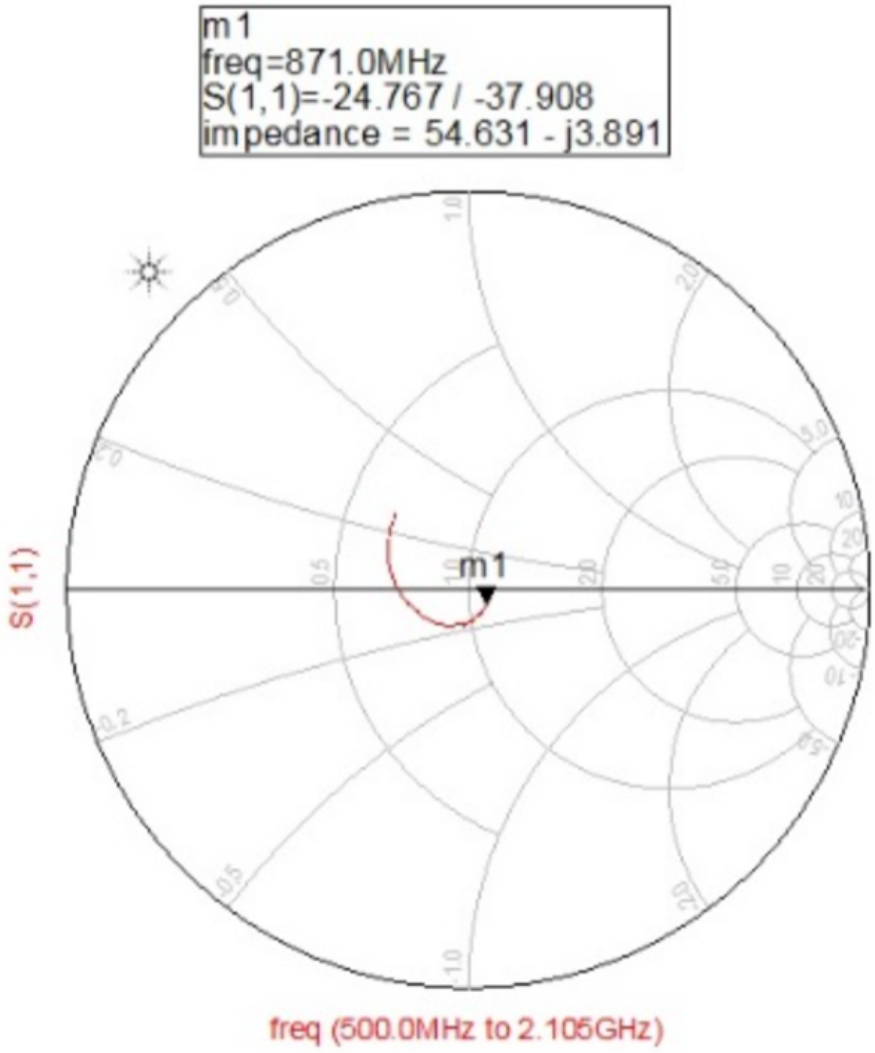

Figure 4.5 ACUT Return Loss

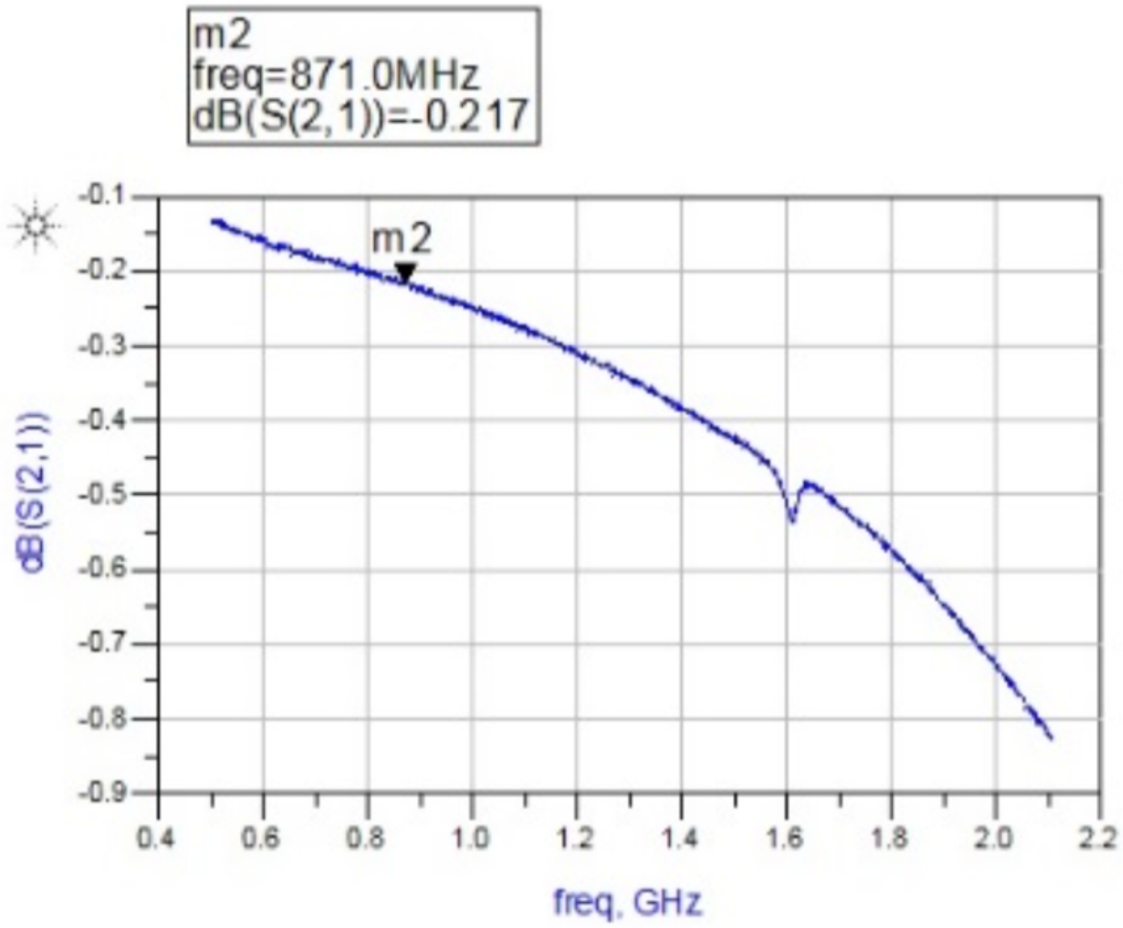

Figure 4.6 ACUT Insertion Loss

4.6.2 Baseline Intermodulation Distortion

The baseline IMD of the setup was measured without the ACUT. Figure 4.7 below shows the measurement points. The baseline IMD level was measured to be below -95 dBm. Figure 4.8 shows the spectrum of the baseline measurement.

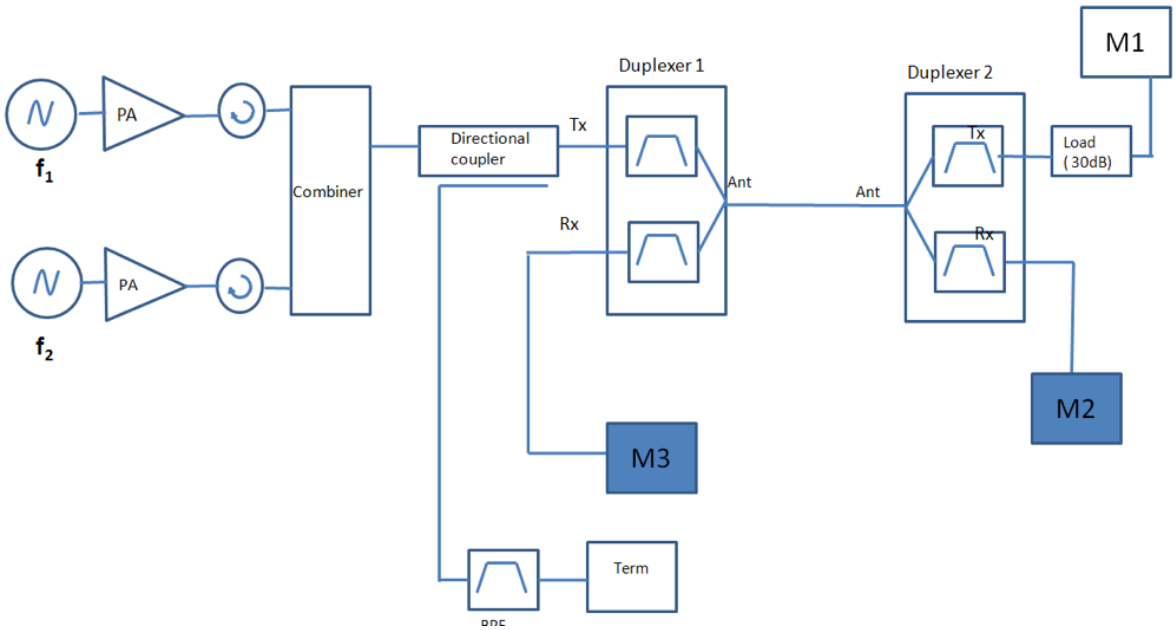

Figure 4.7 Baseline (Setup) IMD Measurement Point

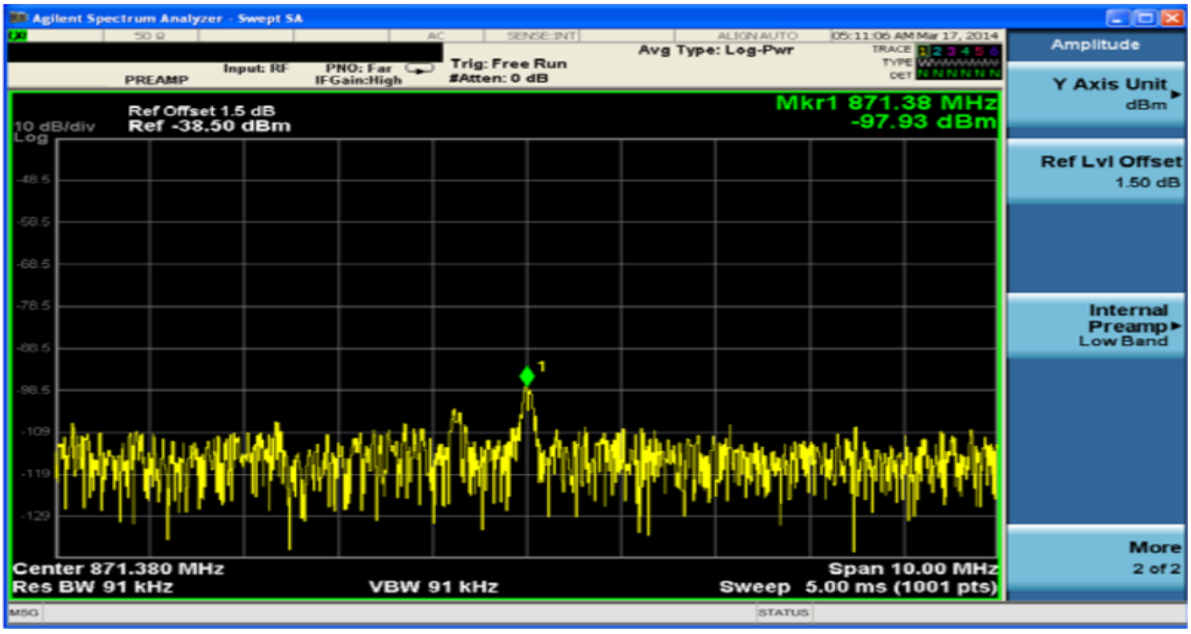

Figure 4.8 Baseline Measurement Spectrum

4.6.3 Power Output

The ACUT fundamental tone power was measured at 23.5 dBm. Figure 4.9 shows the measurement point and the fundamental tones. Figure 4.10 displays the spectrum capture.

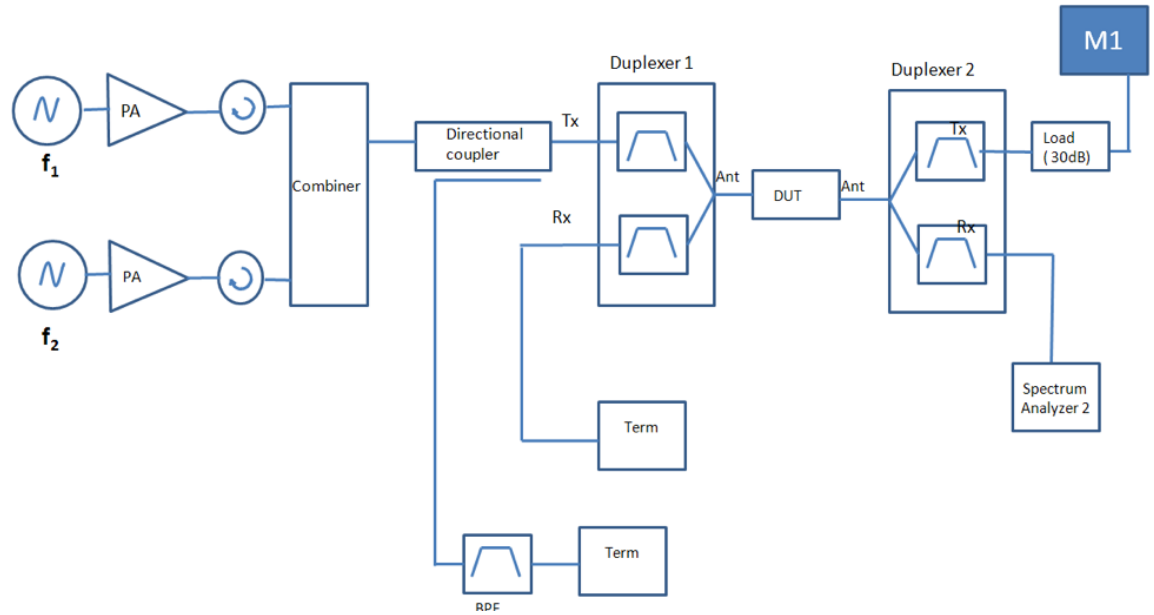

Figure 4.9 ACUT Output: Fundamental Power Constant Monitoring Point

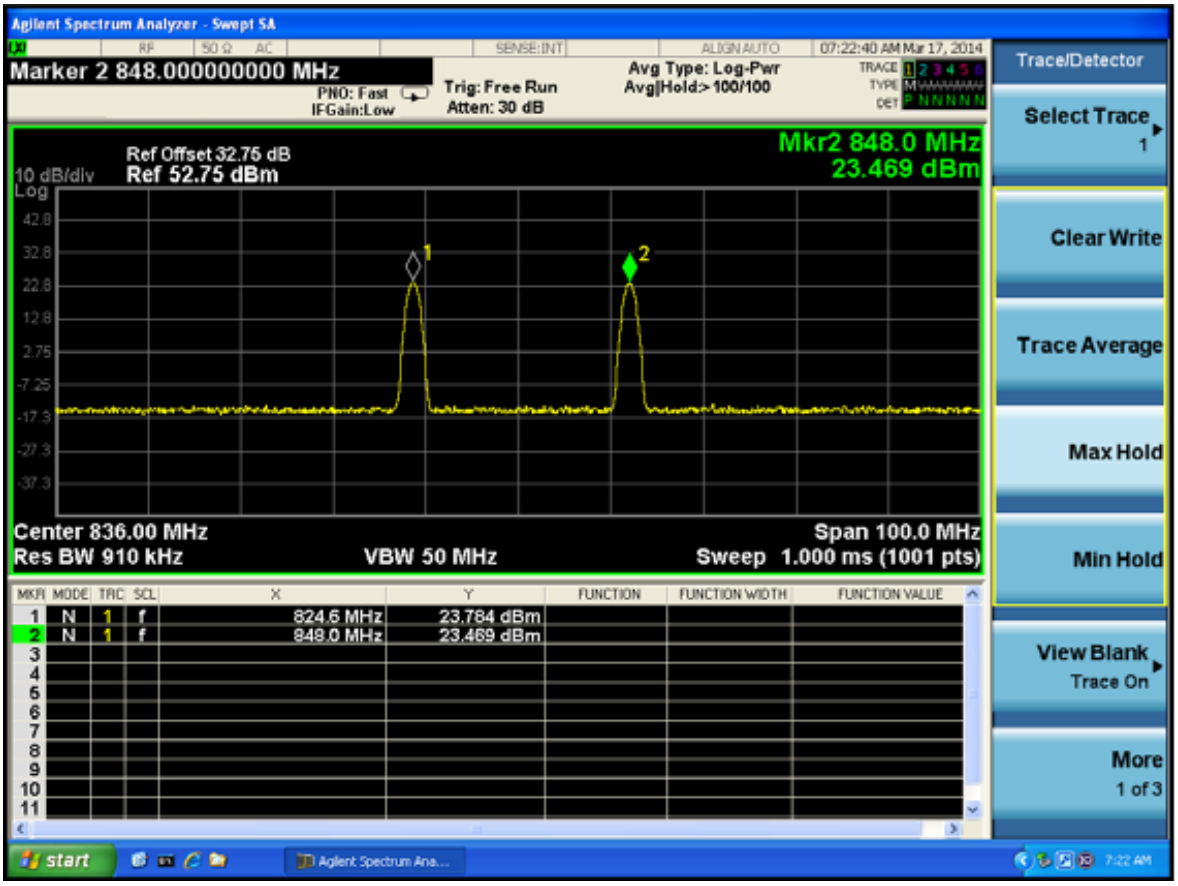

Figure 4.10 ACUT Output: Fundamental Power Output

4.6.4 Forward Intermodulation Distortion

Forward IMD was measured at about -68 dBm. Figure 4.11 shows the measurement point, and Figure 4.12 displays the spectrum capture.

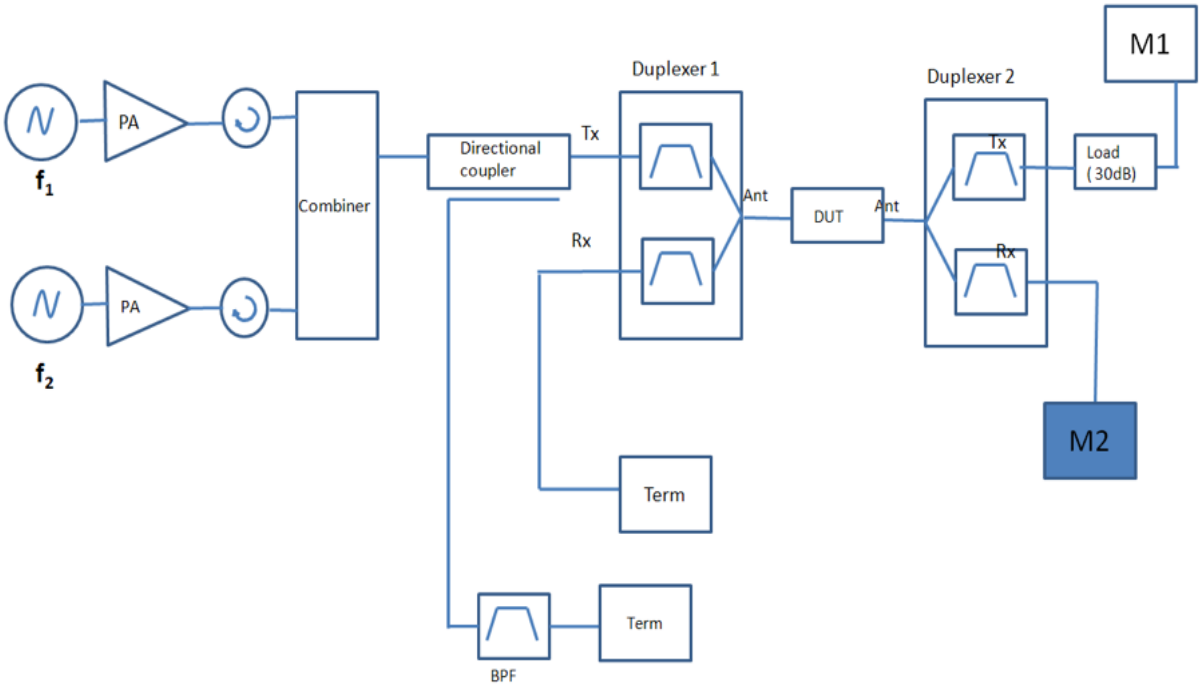

Figure 4.11 Forward IMD Measurement Point

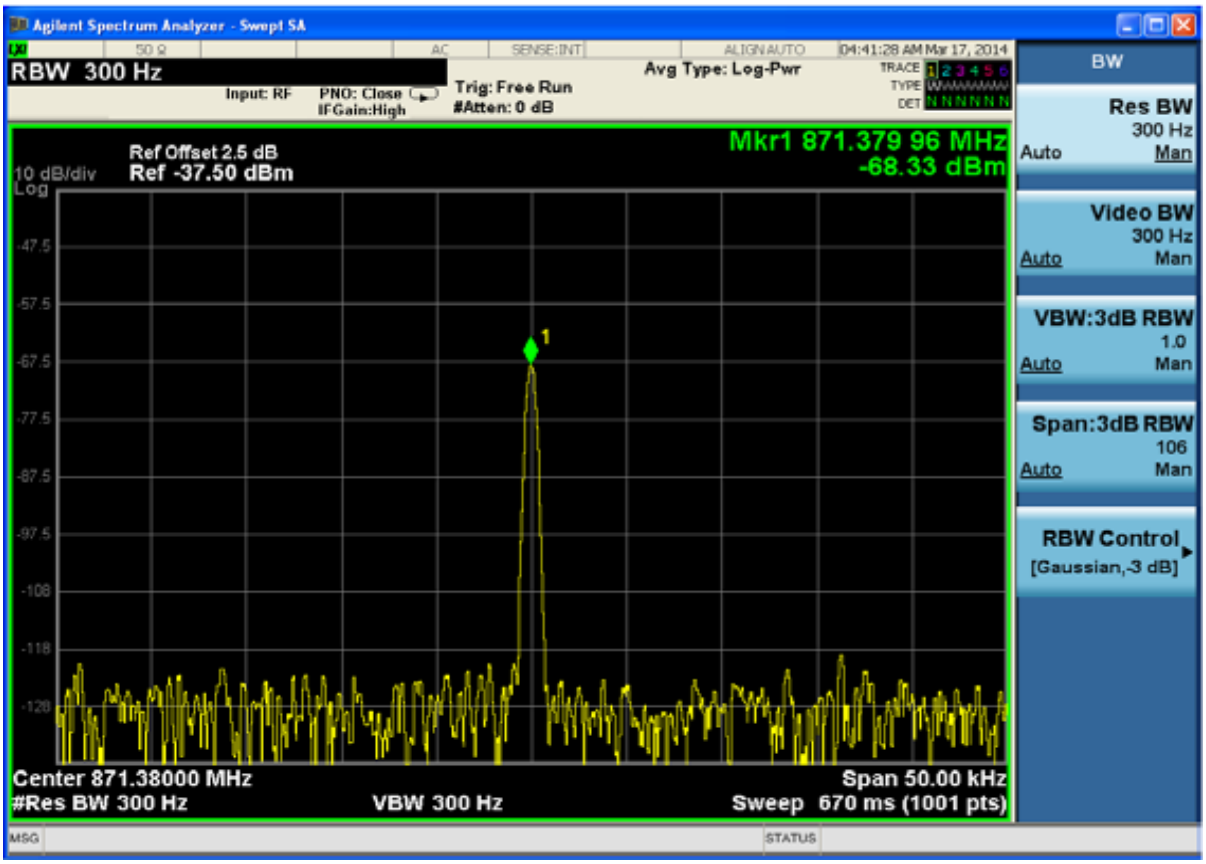

Figure 4.12 Forward IMD Measurement Spectrum

4.6.5 Reversed Intermodulation Distortion

The reversed IMD was measured to be around -65 dBm. Figure 4.13 below, shows the measurement point and Figure 4.14 shows the spectrum capture.

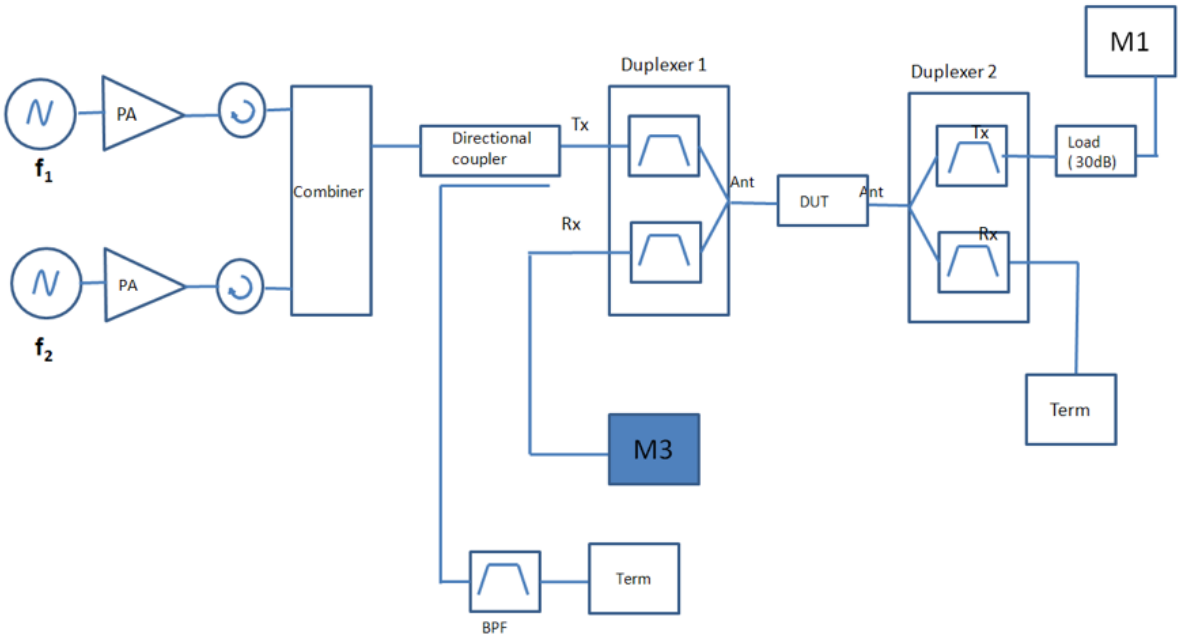

Figure 4.13 Reverse IMD Measurement Point

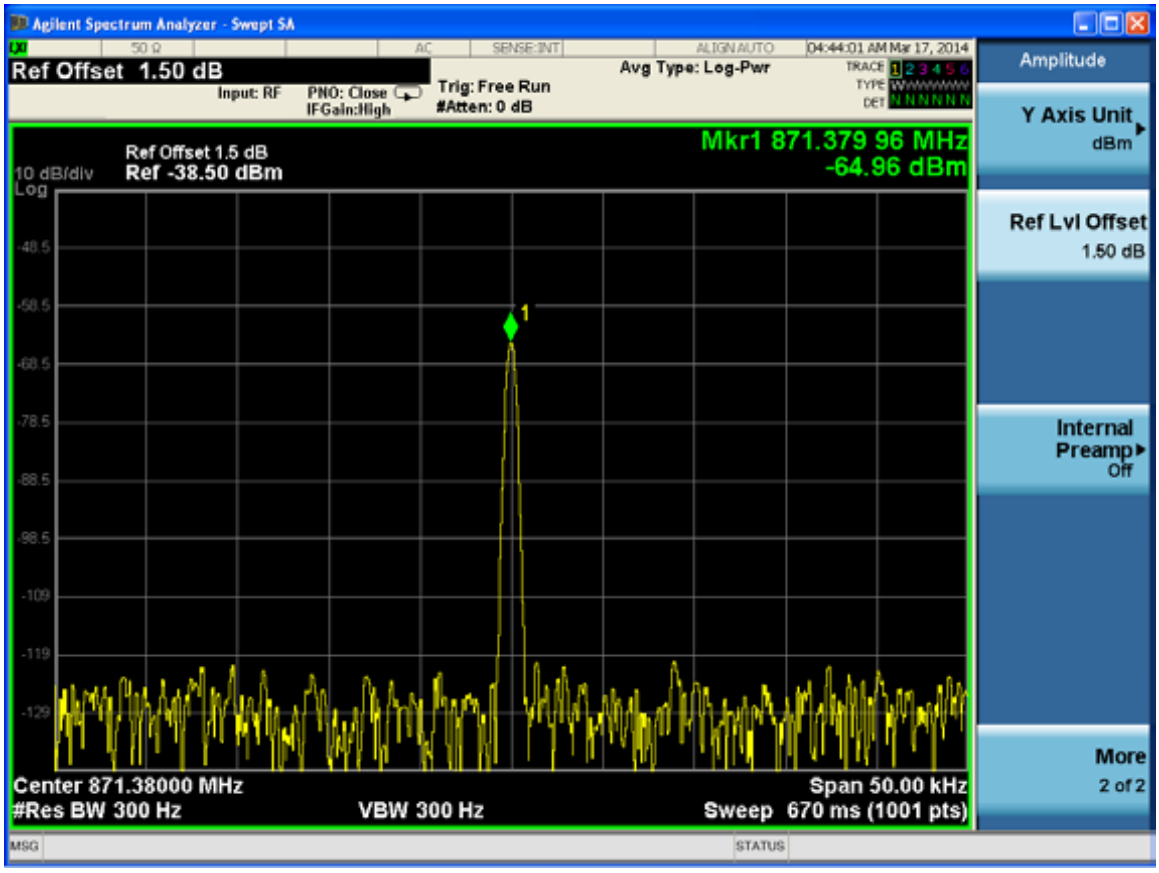

Figure 4.14 Reverse IMD Measurement Spectrum

4.7 Observations from Measurements

IMD is intermittent in nature. The IMD level fluctuates as a function of time and pressure. Pressure was found to be a critical variable. By simply pressing the contact with a nonconductive plastic material (without changing impedance), the IMD level was observed to vary by 20 dB. This observation is very important, since in large product lots, pressure cannot readily be controlled or made constant across millions of units. This could translate to a large variation among units and yield loss.

4.8 Nonlinear Analysis Strategy

Based on the measurement data, it was concluded that PIM can be the dominating nonlinear source in low-profile handheld devices. The next step in the experiment was to perform large signal S-parameter analysis to correlate the IMD data with S-parameters when receiving different input power levels from the VNA. Figure 4.15 shows the method flow.

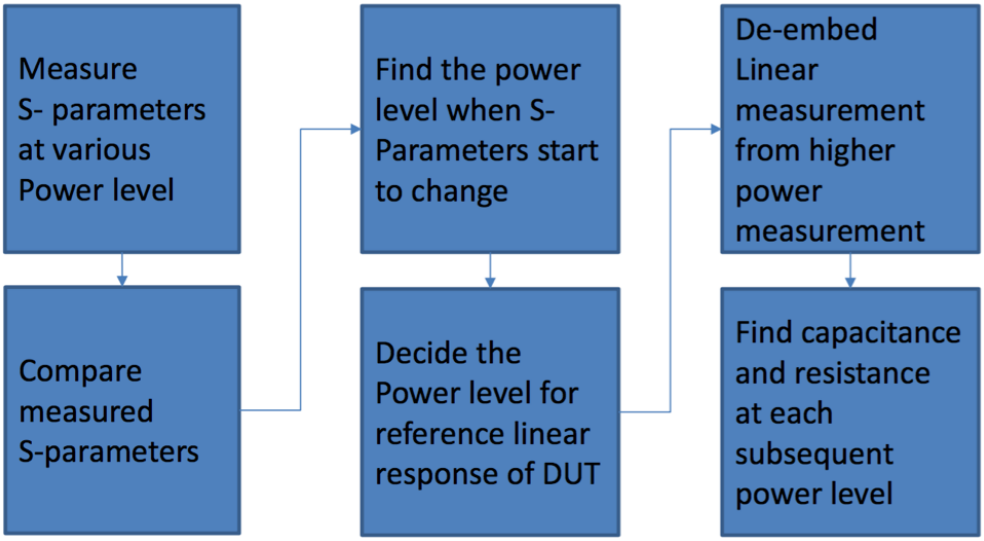

Figure 4.15 Strategy of Nonlinear Analysis

4.9 Large Signal S-Parameter Measurement Methodology

- S-parameters were measured for different power levels (-10 dBm to +13 dBm)
- Maximum power level was restricted to a VNA accuracy level of not more than 13 dBm
- VNA was calibrated separately at all measured power levels
- On the same PCB as the ACUT, a through line was designed
- Through line measurement was used as a baseline to find the VNA response variation up to +13 dBm

4.10 Through Line Large Signal S-Parameters

The measured S-parameters of the through line showed consistent values across different input power levels. Measured S-parameter showed consistent values across different input power levels. Figure 4.16 shows the results.

Power Level (dBm)	S_{11} @ 1GHz (dB)	S_{12} @ 1GHz (dB)
-5	-23.525	-.183
0	-23.308	-.194
5	-22.788	-.201
8	-23.079	-.209
10	-22.373	-.218
12	-21.787	-.230

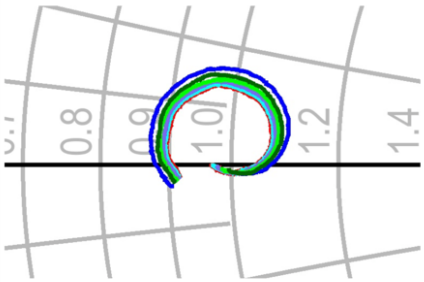

Figure 4.16 Reference Through Line S-Parameters as a Function of Input Power

4.11 Antenna Contact Large Signal S-Parameters

ACUT S-parameters were also measured. S-parameters were measured immediately after the IMD measurement. No significant delta was observed up to 0 dBm. The results are displayed in Figure 4.17.

Power Level (dBm)	S_{11} @ 1GHz (dB)	S_{12} @ 1GHz (dB)
-5	-23.543	-.255
0	-23.761	-.250
5	-24.105	-.255
8	-24.528	-.254
10	-25.293	-.263
12	-26.596	-.264
13	-28.407	-.294

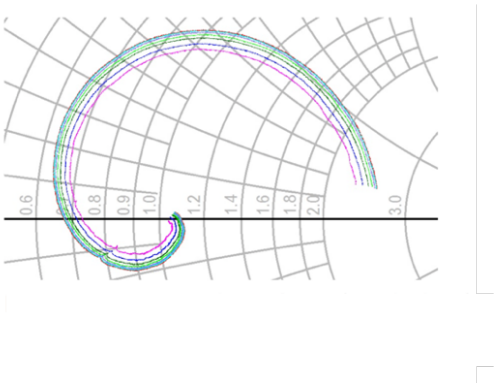

Figure 4.17 ACUT S-Parameters as a Function of Input Power

4.12 Limitations and Future Work

The experiment faced a few limitations when conducting the large signal S parameter measurement. In a typical mobile phone, the conducted transmit power would be higher than 20 dBm, in the case of the GSM band, it would be as high as 33 dBm.

Unfortunately, for this experiment, the VNA transmit power was limited to 13 dBm. In order to correctly correlate the nonlinear behavior, it would be necessary to input power levels equal to those used for the IMD measurements (i.e., 25 dBm). The transmit power can be enhanced by adding an external power amplifier, located at the VNA output. Unfortunately, such an external power amplifier was not available. Once power amplifier is added at the VNA output, the next level of challenge would be to make sure VNA is operated at its linear region. Depending on the VNA linearity and the required dynamic range of measurement, additional filtering might be necessary to be added for the linear operation of the VNA. Modeling nonlinearity therefore turned out to be beyond the scope of this thesis.

This would be an interesting experiment to conduct in the future, and would provide enough information for nonlinear modeling. Sufficient nonlinear modeling would provide the level of understanding needed to analyze the nature of nonlinearity and take the necessary steps to solve the PIM problem.

Chapter 5
Conclusion

Passive intermodulation has been a common problem in high power applications. Through this work it was shown that because of the significantly different material structure, PIM can also be an issue for low-power, low-profile devices. If the frequency combination fits, this can cause significant receiver sensitivity degradation.

Engineers are quite familiar with the active nonlinear sources and adequate filtering are being used to resolve this issue. However, as we have discussed above, PIM generation can occur anywhere within the device. This makes it extremely difficult to locate the source and at the same time makes it a very interesting problem to solve. The purpose of this work was not to solve the problem, but to open the gate for further analysis and future research. A Setup diagram with state-of-the-art measurement equipment was presented and issues related to measurements were discussed. Necessary considerations on designing test fixture and ACUT were also discussed. This will be useful for people who are designing conductive materials such as conductive foam, conductive fabric, RF contacts and modular antennas to characterize or measure nonlinear parameters. Full wave simulation was done to validate ACUT linear response. Circuit simulation was done to find out system dynamic range. Based on this simulation, an ACUT was fabricated and the test fixture was prototyped.

The careful setup design, measurement and simulation have provided the necessary foundation for continued research into PIM and find a standardized solution for Design-for-Coexistence platforms.

Bibliography

[1] qualcomm, “Qualcomm Snapdragon X16 LTE.” [Online]. Available: https://www.qualcomm.com/products/snapdragon/modems/4g-lte/x16. [Accessed: 11-Feb-2016].

[2] “Telecommunications Service Revenue Since 2005.” [Online]. Available: http://www.statista.com/statistics/268636/telecommunications-services-revenue-since-2005-by-region/.

[3] “Nokia Lumia.” [Online]. Available: http://www.gsmarena.com/nokia_lumia_1020-5506.php.

[4] Z. Jing, A. Waltho, Y. Xue, and G. Xingang, “Multi-radio coexistence: Challenges and opportunities,” in *Proceedings - International Conference on Computer Communications and Networks, ICCCN*, 2007.

[5] etsi, “EUROPEAN TELECOMMUNICATION European digital cellular telecommunications system (Phase 2); Full rate speech transcoding,” 1994. [Online]. Available: http://www.etsi.org/deliver/etsi_i_ets/300500_300599/300577/01_60/ets_300577e01p.pdf.

[6] 3GPP, “ETSI TS 136 104.” [Online]. Available: http://www.etsi.org/deliver/etsi_ts/136100_136199/136104/09.04.00_60/ts_136104v090400p.pdf.

[7] P. L. Lui, “Passive intermodulation interference in communication systems,” *Electron. Commun. Eng. J.*, vol. 2, no. 3, p. 109, 1990.

[8] J. H. and F. D. C. M. Kudsia, K. R. Ainsworth, “A High Power Low Passive Intermodulation (PIM) UHF Duplexer for Space Application,” pp. 1–3.

[9] S. K. Baghel, M. A. Ingale, and G. Goyal, “Coexistence possibilities of LTE with ISM technologies and GNSS,” in *2011 National Conference on Communications (NCC)*, 2011, pp. 1–5.

[10] X. Yang, H. Y. Liu, and X. Guo, “Bluetooth coexistence with 4G broadband wireless networks,” in *SECON 2010 - 2010 7th Annual IEEE Communications Society Conference on Sensor, Mesh and Ad Hoc Communications and Networks*, 2010.

[11] A. Teković, I. Pešut, and Z. Morić, “Voice Service in an LTE Network- CSFB,” no. September 2013, pp. 25–27, 2014.

[12] Z. Hu, R. Susitaival, Z. Chen, I. K. Fu, P. Dayal, and S. Baghel, “Interference avoidance for in-device coexistence in 3GPP LTE-advanced: Challenges and solutions,” *IEEE Commun. Mag.*, vol. 50, no. 11, pp. 60–67, 2012.

[13] L. H. Li, F. L. Lin, and H. R. Chuang, “Complete RF-system analysis of direct conversion receiver (DCR) for 802.11a WLAN OFDM system,” *IEEE Trans. Veh. Technol.*, 2007.

[14] B. Leung, *VLSI for Wireless Communication*. Boston, MA: Springer US, 2011.

[15] F. Ramian, “Intermodulation Distortion Measurements on Modern Spectrum Analyzers Application Note,” 2012. [Online]. Available: https://cdn.fswwwp.rohde-schwarz.com/pws/dl_downloads/dl_application/application_notes/1ef79/1EF79_1E.pdf.

[16] S. Saha, “RF Front-End Design for X Band using 0.15µm GaN HEMT Technology,” University of Ottawa, 2016.

[17] Bluetooth, “Specification of The Bluetooth System,” *T O C*, 2010. .

[18] A. Sedra and K. Smith, *Microelectronic Circuits*, 7th ed. oxford: Oxford University Press, 2015.

[19] S. Yan, C. F. Wang, J. Kotulski, and J. M. Jin, “Time-domain finite element analysis of ferromagnetic hysteresis in three dimensions,” in *IEEE Antennas and Propagation Society, AP-S International Symposium (Digest)*, 2014.

[20] Alan Seabaugh, “The Tunneling Transistor,” *IEEE Spectrum*. [Online]. Available: spectrum.ieee.org/semiconductors/devices/the-tunneling-transistor. [Accessed: 31-Jul-2017].

[21] “Electromagnetic Radiation (a.k.a. Light).” [Online]. Available: http://abyss.uoregon.edu/~js/ast123/lectures/lec06.html.

[22] R. a. Serway, C. J. Moses, and C. a. Moyer, *Modern Physics*, 3rd ed. Belmont: Brooks Cole, 2005.

[23] N. Zhang, W. Cui, and T. Hu, “Passive Intermodulation Analysis for Mesh Antennas,” in *IEEE Antennas and Propagation Magazine*, 2015, no. 4th Asia-Pacific Conference.

[24] C. Rowell and E. Y. Lam, “Mobile-phone antenna design,” *IEEE Antennas Propag. Mag.*, 2012.

[25] B. C. Kim, J. H. Yun, and H. Do Choi, “Small wideband PIFA for mobile phones at 1800

MHz," in *2004 IEEE 59th Vehicular Technology Conference. VTC 2004-Spring (IEEE Cat. No.04CH37514)*, 2004, vol. 1, p. 27–29 Vol.1.

[26] A. F. Molisch, Wireless Communications, 2nd ed. Wiley.

[27] D. A. Sanchez-Hernandez , Multi Band Integrated Antennas for 4G Terminals, 1st ed. Artech House Inc, 2008.

[28] N. L. Bohannon and J. T. Bernhard, "Ground plane effects on planar inverted-F antennas," in IEEE Antennas and Propagation Society, AP-S International Symposium (Digest), 2012.

[29] ifixit, "Samsung Galaxy Note Antenna Replacement." [Online]. Available: https://www.ifixit.com/Guide/Samsung+Galaxy+Note+Antenna+Replacement/14379.

[30] ifixit, "BlackBerry Bold 9000 Antenna Replacement." [Online]. Available: https://www.ifixit.com/Guide/BlackBerry+Bold+9000+Antenna+Replacement/8138#s33007.

[31] C. A. Balanis, *Antenna Theory: Analysis and Design*, 3rd ed. Wiley-Interscience.

[32] wiki, "FR-4." [Online]. Available: https://en.wikipedia.org/wiki/FR-4. [Accessed: 01-Jul-2017].

[33] Anon, "Understanding power splitters," *Electron. World*, vol. 105, no. 1753, pp. 45–46, 1999.

[34] "WiKi PS." [Online]. Available: https://en.wikipedia.org/wiki/Microwave_power_meter.